# A MULTIPHYSICS MODEL FOR CARBON NANOTUBE BASED NANOELECTROMECHANICAL CONTACT SWITCH

**Yihan Nie**

**Bachelor of Mechanical Engineering**

Principle supervisor: Yuantong Gu

Associate supervisor: Haifei Zhan

Emilie Sauret

Submitted in fulfilment of the requirements for the degree of

Master of Philosophy

School of Chemistry, Physics, and Mechanical Engineering

Science and Engineering Faculty

Queensland University of Technology

2018

# Keywords

Nano Electromechanical System

Multiphysics Modelling

Molecular Dynamic

Grand Canonical Monte Carlo Method

Dynamic Electric Field

Gas Adsorption

Vibration

Carbon Nanotube

# Abstract

With the scaling down of the size of electronic devices, the traditional transistor structure is approaching its physical limit. To meet the property requirements for an electronic device at the nanoscale, researchers have proposed several new structural designs. The nanoelectromechanical contact switch (NEMCS) is one such device, which has been fabricated and tested in laboratories using carbon nanotubes (CNT) or other one-dimensional nano structures. However, the nano switches made in laboratory are not always reliable and have many failure scenarios, which require extensive tests to identify and avoid. Since the nanoscale experiments are large consumers of time and resources, numerical simulation can be applied to design the nano switch in a more effective and efficient way.

The NEMCS system involves multiple physical phenomena, including force, thermal, electric and fluid environments, which require multiphysical modelling to describe the system properly. As many physical laws at the macroscale fail to give a proper prediction at the nanoscale, in this work, a multiphysics molecular model for a CNT-based NEMCS has been developed, and its dynamic properties have been investigated on the basis of molecular dynamic simulation, combining the atomistic moment method for electric field simulation, and the grand canonical Monte Carlo method for adsorption simulation. By updating the charge information, the dynamic electrical field provides a better result than the static results achieved previously. Also, the adsorption on the inside surface and outside of CNT has different structures, and the vibration properties respond differently to changes in the environment.

The developed model can predict an accurate pull-in voltage and other dynamic properties of NEMCS working in a vacuum without a geometric restriction for the system. For the NEMCS working in a gaseous environment, such a model can also predict the damping ratio and frequency. These two features can guide the design of NEMCS in the future.

# Table of Contents

# List of Figures

# List of Abbreviations

| | |
|---|---|
| AFM | Atomic Force Microscope |
| AIREBO | Adaptive Intermolecular Reactive Empirical Bond Order |
| AMT | Atomistic Moment Theory |
| BEM | Boundary Element Method |
| BWR | Blue-White-Red |
| CMOS | Complementary Metal-oxide Semiconductor |
| CNT | Carbon Nanotube |
| DFT | Density Function Theory |
| EBT | Euler-Bernoulli beam theory |
| EOS | Equation of Statue |
| FDM | Finite Difference Method |
| FET | Field-effect Transistors |
| FIB | Focused Ion Beam |
| GCMC | Grand Canonical Monte Carlo |
| HPC | High Performance Computer |
| IAST | Ideal Adsorbed Solution Theory |
| IC | Integrated Circuit |
| ITRS | International Technology Roadmap for Semiconductors |
| LAMMPS | Large-scale Atomic/Molecular Massively Parallel Simulator |
| LDM | Logarithmic Decrement Method |
| LJ | Lennard-Jones |
| LTI | Linear Time Invariant |
| MD | Molecular Dynamic |
| MEMS | Microelectromechanical System |
| MtM | More than Moore |
| NEMCS | Nano Electromechanical Contact Switch |
| PBS | Portable Batch System |
| RDF | Radial distribution function |
| REBO | Reactive Empirical Bond-order |
| S-G filter | Savitzky-Golay FIR Smoothing Filter |
| SEM | Scanning Electron Microscope |
| STFT | Short-time Fourier Transform |
| SWCNT | Single Wall Carbon Nanotube |
| TBT | Timoshenko Beam Theory |
| TEM | Transmission Electron Microscope |
| TLS | Two Level System |
| VMD | Visual Molecular Dynamics |

# Statement of Original Authorship

The work contained in this thesis has not been previously submitted to meet requirements for an award at this or any other higher education institution. To the best of my knowledge and belief, the thesis contains no material previously published or written by another person except where due reference is made.

Signature: QUT Verified Signature

Date: 22 / 10 / 2018

# Acknowledgements

Thanks for the advice and kind help both in research and life from my supervisor team: Yuantong Gu, Haifei Zhan, and Emilie Sauret.

Thanks for the help and support from people in Laboratory for Advanced Modelling and Simulation in Engineering and Science (LAMSES), especially the nano subgroup.

Thanks for my parents who give the financial support as well as the spiritual encouragement.

The MD and GCMC simulation used Large-scale Atomic/Molecular Massively Parallel Simulator (LAMMPS) code package developed by Sandia National Laboratories.

The computer simulation used the resource from High Performance Computer (HPC) from Queensland University of Technology.

Thanks to Dr Christina Houen of Perfect Words Editing for editing and proofreading my thesis, according to the guidelines of the university and of the Institute of Professional Editors (IPEd).

# Publications

- Yihan Nie, Haifei Zhan, Zhuoqun Zheng, Arixin Bo, Edmund Pickering, and Yuantong Gu, "*Significant impacts of gas adsorption on the performance of carbon nanotube resonator*" (To be submitted to *Nanotechnology*).
- Yihan Nie, Haifei Zhan, Zhuoqun Zheng, Arixin Bo, Edmund Pickering, and Yuantong Gu, "*Effects of changing electrical field on the vibrational properties of carbon nanotube*" (To be submitted to *Applied Physics Letters*).
- Zhuoqun Zheng, Haifei Zhan, Yihan Nie, Xu Xu, and Yuantong Gu, "*General Existences of Two-dimensional Resonance of Nanowires"* (To be submitted to *ACS Nano*).
- Yihan Nie, Haifei Zhan, Arixin Bo, Yuantong Gu, "*Simulation of dynamic response of carbon-nanotube based electromechanical switch in atmosphere*", oral presentation in *ACCM-3 2018 Conference*.
- Yihan Nie, Haifei Zhan, Arixin Bo, Yuantong Gu, "*Molecular dynamic simulation of carbon nanotube-based electromechanical switch with dynamic electric field*", poster presentation in *NanoS-E3 2017 Conference*.

# Chapter 1: Introduction

In this chapter, Section 1.1 presents the background of experimental and numerical studies of nanoelectromechanical contact switches as well as the research problems; the following section states the objectives of developing a new multiphysics model for NEMCS (Section 1.2). Section 1.3 highlights the significance of developing this new multiphysics model, and gives definitions used in this research. Finally, Section 1.4 outlines the structure of the remaining chapters.

## 1.1 BACKGROUND AND RESEARCH PROBLEM

The energy efficiency of traditional transistors drops fast in the sub-100 nanometre regime, because of the increase of threshold leakage and gate leakage [1], which limits the scaling of the processor design. One way to overcome this restriction is to retain the structure of traditional transistors and find new materials to improve performance on a smaller scale; another is to design a new structure, which can work more efficiently with the scaling of the system. The nanoelectromechanical contact switch (NEMCS) is designed on a scaling microelectromechanical system (MEMS) based on the mechanical and electrical properties of nano structures. A carbon nanotube can be used to build the NEMCS, because it has high theoretical mechanical properties and variable electrical performance. With the help of a scanning electron microscope (SEM), and a focused ion beam (FIB), individual NEMCSs with a carbon nanotube as a moveable part can be easily fabricated. However this process requires a lot of time and resources. For optimising the geometry and structure design, a computational method can be an efficient way to find the appropriate design to achieve the required properties and guide the experimental work and fabrication. To model the NEMCS appropriately, multiple physical fields need to be taken into consideration. Coupled with the bending and vibration of moveable parts, the electric field, charge distribution, adsorption phenomenon, and fluid drag force, cannot be ignored. In the holding process of NEMCS, the Joule heating process and the thermal field can also influence the performance, and are the main factors that can cause failure [2]. The model, including multiple physical phenomena and their coupling relations, is called a multiphysics model, and is becoming an essential method for computational work to

achieve a result close to reality. A multiphysics model for NEMCS is still a gap for researchers to fill.

For the nano structures, classic beam theory, based on the continuum assumption of materials and ignoring the surface effect, can result in large differences from reality. One of the common approaches to studying the mechanical property of nano structures is molecular dynamic (MD) simulation, which looks at the atomic level and describes the relationships between atoms with empirical potentials or force fields. The MD model of carbon nanotube-based NEMCS has been proposed in previous research [3]–[5]. However, the distribution of charges on each atom in the MD model is static, and is set without theoretical calculation in most cases, which does not reflect the actual situation. A theoretical calculation on the charge distribution in the system combined with MD simulation is one major part of the multiphysics model of NEMCS that remains to be solved.

Another physical factor in NEMCS is the working environment. Because the fabrication and testing of these nano devices usually need the aid of SEM and FIB, the working performance is achieved under vacuum conditions, and most simulations have applied their working conditions as a vacuum [2], [6]. However, the performance of NEMCS in a real situation (under atmosphere) still needs to be investigated, for it is expected to deviate from the case under vacuum conditions. If NEMCS can work well in a gaseous environment, the package cost will be reduced and the applications will be broadened. Additionally, computational efficiency is one of the concerns in choosing the building blocks of processors. The working frequency of the commercialised processor has reached GHz. For nanowires and nanotubes, one of the strengths of building a nano resonator is that it has a high quality factor and low damping ratio. When it comes to NEMCS with high computing frequency, such strength can become a drawback. With low damping, when the NMECS is switched off, the movable part will continue vibrating for a long time, and interfere with the later output of the signal. Thus, NMECS with damping is worthy of investigation for high computing frequency, and a gaseous environment is expected to provide the required damping for the system. Apart from NEMCS, the vibration damping of nano structures in fluid has more applications, such as the design of gas sensors and atomic force microscope (AFM) work in a fluid environment.

In conclusion, building a multiphysics model for NEMCS, including a dynamic electric field and a gaseous environment, can be useful for the accurate interpretation of its working mechanism, expanding the working environment to an atmospheric one, and improving the performance with a tuneable damping ratio for high frequency processing. The simulation results can also be useful for other similar devices with 1D nano structural vibration characteristics.

To achieve this, the following major research questions need to be solved:

- What are the gas adsorption configurations of the CNT in different gaseous environments, and how can they be combined with the vibration simulation to see the influence of adsorption on vibration properties?
- How to calculate the dynamic charge distribution along the moveable CNT and the fixed electrode, and how to couple it with MD model for NEMCS?

## 1.2 OBJECTIVES

To establish a more accurate model for NEMCS and thus enable high fidelity prediction and analysis, in this research, a multiphysics model is developed, including a dynamic electric field and gaseous environment, and considering the charge distribution and adsorption phenomenon. The CNT-based NEMCS is taken as the representative system, which will be used to analyse the dynamic response of NEMCS in a gaseous environment. The objectives of developing this multiphysics model are as follows:

- To simulate the adsorption properties of CNT in a gaseous environment, and investigate the influence of adsorption on CNT vibration properties of the NEMCS moveable part.
- To calculate the dynamic charge distribution during the pull-in process in the NEMCS system, and investigate the dynamic response of the system.

## 1.3 SIGNIFICANCE, SCOPE AND DEFINITIONS

Generally speaking, building a multiphysics model can give an accurate prediction of the properties of NEMCS compared to previous models, and thus help to optimise the geometry and material design of the NEMCS with less cost compared to

the experimental way. The result can also guide further experimental work, explain some of the failure scenarios detected, and propose possible solutions to avoid such failures. In the multiphysics model, the precise electric field and the gaseous environment will be included. To study the dynamic properties of the moveable part in NEMCS, the dynamic electric field should be taken into consideration, but has been neglected in previous work. The gaseous environment case study can also expand the working environment of NEMCS and reduce the package cost. The damping effect brought by the gases can be useful for the NEMCS with high frequency input; however, previous studies focus on the pull-in process and response time, whereas the pull-out process and the recovery time have rarely been discussed. The developed model can extend to other devices with similar structures and help their design; for example, gas sensors, and AFM tips working in a fluid environment.

Based on MD simulation, the multiphysics model being developed is more suitable for a nanoscale system than the classic beam and fluid theory with continuum assumption. Since, so far, there is no mature software to calculate the dynamic electric field coupled with the motion of atoms at a nanoscale, part of the codes have to be developed originally. The atomistic moment theory (AMT) used for the electric field study can provide results close to the predictions from density function theory (DFT) calculations, and requires less computational time and resources. The dynamic electric field is calculated using an AMT and MD combined method, which is essential, but neglected in most studies of the dynamic response of NEMCS [3]–[5]. For the adsorption-vibration model in a gaseous environment, as the adsorption is significant for nano structures, the simulation result for adsorption is important, and can affect the final conclusion. Previous studies for vibration in fluids used continuum assumptions and did not consider the adsorption phenomenon, which is not suitable for an NEMCS system [7], [8]. The grand canonical Monte Carlo (GCMC) method combined with MD simulation is adopted in this research, which can mimic the adsorption phenomenon under certain temperatures and pressures. The adsorption-vibration model can also be applied to other nano structures for vibration in fluids.

In the developing multiphysics model for NEMCS, the dynamic electric field and fluid field in the system are relevant to the pull-in process (when the voltage is applied, and the NEMCS switched on) and the pull-out process (when the voltage is reset, and the NEMCS switched off). The thermal field in the system is not included

in the study, because its influence on the system is not significant in these two processes.

Compared with previous models established by other researchers [9], [10], the multiphysics model being built has the following improvements:

- An adsorption-vibration model for the CNT moveable part can be used to study the damping effect of the NEMCS moveable parts and other devices with similar structures in a gaseous environment.
- It provides a more accurate setting for the charge distribution, and can have a better description for the dynamic response for CNT moveable parts in the NEMCS pull-in process.

## 1.4 THESIS OUTLINE

The previous research works and the classic theories on NEMCS, electric field, adsorption, and vibration will be introduced in Chapter 2. Chapter 3 presents a detailed simulation design, and describes how the data will be processed to get a final result. Chapter 4 presents the results for the adsorption and vibration model, and discusses the results. Chapter 5 shows the results for dynamic electric field simulation in NEMCS, and discusses the results in detail. Finally, the conclusions and the limitations of this work will be summarised for future work in Chapter 6.

# Chapter 2: Literature Review

In this chapter, the historical background of scaling down of electronic devices will be introduced (Section 2.1). Then, the literature will be reviewed on the following topics: basic knowledge about NEMCS (Section 2.2); molecular dynamic simulation and its use in previous NEMCS simulation (Section 2.3); the simulation of the electric field in nanostructures (Section 2.4); adsorption simulation for nanostructures (Section 2.5); and the vibration test for nanostructures (Section 2.6). Section 2.7 presents the implications of developing a multiphysics model from the literature.

## 2.1 HISTORICAL BACKGROUND

People have benefited a lot from the miniaturisation of electronic devices, from the convenience of transport to the reduction of manufacturing costs. For the past 50 years, the complexity of circuits has doubled every two years, as Gordon Moore predicted in 1975 [11]. This was accomplished by the improvement of transistor technology and scaling of its geometric size: the vacuum tubes used in the 1940s were replaced by bipolar transistors, which were later replaced by field-effect transistors (FET). However, such growth trends can no longer be expected after 2010, with current knowledge of complementary metal-oxide semiconductors (CMOS). After 2013, the Moore's Law rate slowed to three years, to double the number of transistors on chips [12], approaching the fundamental thermal limits of some integrated circuits (IC). The energy dissipation caused by the subthreshold leakage and gate leakage in transistors lowers the efficiency of ICs. From the international technology roadmap for semiconductors (ITRS), the miniaturisation of the IC can use other technologies than traditional transistors for sophisticated processes, and the integration of multiple heterogeneous technologies to build a smaller IC is called "more than Moore" (MtM).

## 2.2 BASIC KNOWLEDGE ABOUT NEMCS

NEMCS is one of the devices which can be integrated into the design of IC and help to overcome the energy dissipation problem in miniaturising the geometrical size of IC. The NEMCS idea is derived from the micro-electromechanical system (MEMS). With the development of synthesising techniques for different kinds of nano structures,

the fabrication of NEMCS in the laboratory has become possible, many of which were built from CNTs.

### 2.2.1 NEMCS structure and operating principles

The structure of NEMCS can be either simple or complex according to the functions in design. The basic structure of NEMCS has three components: moveable parts, gate electrodes, and drain electrodes. The moveable parts usually are made up from nanowires or nanotube-like 1D structures, which are flexible and can undergo large elastic deformation. The voltage between the moveable part and the gate electrode is the NEMCS input signal, and provides the electrostatic force to bend the moveable part. The drain electrode is the output of the signal to judge whether the switch turns on or not. The gate electrode and the drain electrode can be either separate or together, depending on the NEMCS design, (shown in **Figure 2-1**). The number of gate electrodes and drain electrodes can also be more than one to achieve complex logical calculations. Replacing transistors with the NEMCS in some logical circuits can simplify the IC design. For example, to make a four-terminal XOR gate needs at least ten CMOS transistors, but only two NEMCS [13].

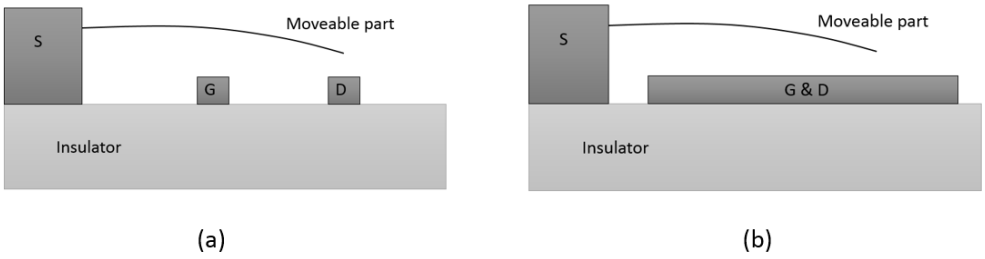


***Figure 2-1*** *The NEMCS structure with: (a) separate electrodes, and (b) combined electrodes. Here, S, G, and D stand for the source, ground, and drain electrode, respectively.*

When the voltage between the gate electrode and moveable part is larger than the elastic restoring force, the moveable part will bend and contact the drain electrode to form a closed circuit. The process for the moveable part bending towards the drain electrode till contact (driven by electrostatic force) is called the pull-in process. When the voltage resets, the restoring force of the moveable part will overcome the stiction force between the contact interface, and the moveable part will go back to the initial balanced state and wait for the next input signal. The process from the separation of

the contact interface to the final balance state of the moveable part is called the pull-out process. The working mechanism of NEMCS determines that the threshold leakage of the device is caused by the thermal motion of the moveable part, which is relatively low compared with the circuit when the moveable part contacts with the drain electrode. This means that the NEMCS has a high on/off ratio.

Apart from the advantages of NEMCS mentioned above, it is also suitable for severe working conditions with radiation, high temperatures, and the external electric field of the working mechanism. NEMCS also consumes less power than the CMOS system to achieve the same goal at low frequency [14].

### 2.2.2 Experimental work on NEMCS

The synthesis of nano structures has brought the NEMCS design into reality, especially when using carbon nanotubes. The individual NEMCS can be fabricated by manipulation under SEM, but reliability is one of the major concerns in experimental work. The high on/off ratio is treated as an advantage in the comparison between NEMCS and a CMOS transistor, but the high current can result in the failure of NEMCS caused by the Joule heating effect when the switch holds on for a long time, which could cause the burning and breaking of the moveable part [2]. Such problems could be solved by the increase of contact resistance between the moveable part and the drain electrode, by replacing the metal electrode with diamond like carbon [2]. The defects in the moveable part can also cause mechanical failure during the repetition of the switch process. To get an NEMCS reliable over a long time run requires the synthesis of defect-free nanostructures. The use of CNT with minimal defects could achieve consistent switching for millions of cycles [15]. Apart from this failure problem, the most common problem is the stiction, which means the moveable part remains attached to the drain electrode after the voltage is reset, because of the adhesion force. A proper geometric design, choice of material, and treatment of the surface can limit such problems, either by reducing the adhesion force, or increasing the elastic restoring force. Another way to solve this problem is to apply another voltage to separate the moveable part and the electrode. Using this kind of design, the NEMCS could operate millions of cycles without stiction failure [16]. Roy et al. discovered that nano-mechanical sensors can improve their properties with large damping, which can be provided by a gaseous environment [17].

Though some of the failure scenarios can be avoided by proper structural design, the NEMCS is still in the laboratory stage, and has a long way to go before industry production. The massive production of NEMCS is still challenging. The experimental testing of the NEMCS is usually in a vacuum, while the actual usage of NEMCS is normally in atmosphere, and NEMCS in atmosphere can have a better performance [17]. This dilemma indicates that many factors influencial on the performance of NEMCS are not considered, like oxidation, adsorption, and other kinds of contamination. The encapsulation of NEMCS will be another issue to investigate on the way to final application. Last but not least, finding a suitable design of NEMCS needs to consider many aspects, which brings different requirements for the design parameters. Such requirements can be contradictory with each other. For example, NEMCS with low pull-in voltage usually have a narrow gap between the moveable part and the electrode, and a flexible moveable part. But such a design is more likely to suffer from the stiction issue. Large contact resistance and small adhesion force also have different requests for the surface roughness of the electrode. The final design needs to compromise with all requirements, and demands extensive and tedious trials, which is time-intensive and expensive from an experimental perspective.

### 2.2.3 Computational work on NEMCS based on classic theories

Since the experimental way to find the best parameters in design is expensive, some models for NEMCS simulation have been put forward by researchers. Generally, all simulation works done previously focused on the pull-in process and computed the pull-in voltage [9], [18]. Two major methods have been adopted, which are classic beam theory based on the continuum, and molecular dynamic simulation. These two methods could also be combined together in a multiscale model for simulation accuracy and efficiency. The following will briefly introduce classic beam theory and compare beam theory-based calculations with MD simulations. A thorough discussion of the molecular dynamic simulation and its use in NEMCS simulation will be presented in Section 2.3.

The basic idea of the modelling is to set the electrostatic force and Van der Waals force as the driving forces in the bending process. According to classic static beam theory, such a relation can be expressed by the following equation:

$$EI\frac{d^4r}{dx^4} = q_{elec} + q_{VdW} \tag{2-1}$$

where $E$ is the Young's modulus of the moveable part, $I$ is the moment of inertia, $r$ is the gap between the moveable part and the electrode, $x$ is the positon along the moveable part, $q_{elec}$ is the electric force on the moveable part per unit length, and $q_{VdW}$ is the Van der Waals force per unit length as shown in **Figure 2-2**.

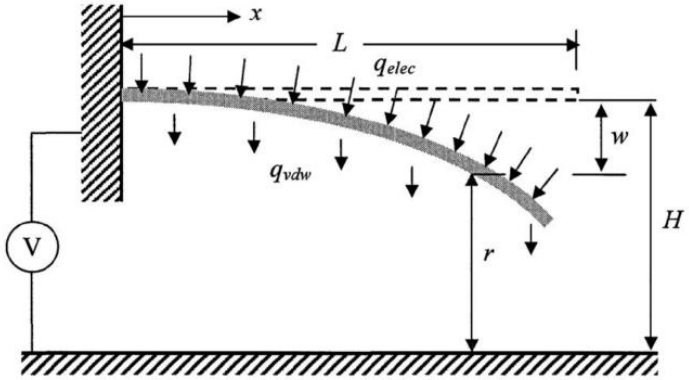


***Figure 2-2*** *A schematic image for NEMCS model* [9].

The above equation could be further improved by finite kinematics [9], and transformed into the following equation:

$$EI\frac{d^2}{dx^2}\left(\frac{\frac{d^2r}{dx^2}}{\left(1+\left(\frac{dr}{dx}\right)^2\right)^{\frac{3}{2}}}\right)=(q_{elec}+q_{VdW})\sqrt{1+\left(\frac{dr}{dx}\right)^2} \tag{2-2}$$

Eq. 2-1 can also be added to the dynamic part on the left side to get [18]:

$$\rho A\frac{\partial^2 r}{\partial t^2}+c\frac{\partial r}{\partial t}+EI\frac{\partial^4 r}{\partial x^4}=q_{elec}+q_{VdW} \tag{2-3}$$

where $\rho$ is the density, $A$ is the cross-section area, $c$ is an assumed constant (suitable for NEMCS with small deflect).

To solve the above equations, the $q_{VdW}$ and $q_{elec}$ need to be calculated. For Van der Waals force, the commonly adopted simulation method uses the Lennard-Jones potential. The potential between the two atoms is:

$$\phi_{ij}=4\varepsilon[(\frac{\sigma}{r_{ij}})^{12}-(\frac{\sigma}{r_{ij}})^{6}] \tag{2-4}$$

where $\varepsilon$ is the depth of the potential well, $\sigma$ is the distance where the potential between particles is zero , and $r_{ij}$ is the distance between two atoms. For the bulk material, the

energy between the two bodies could be calculated through double volume integration [19]:

$$E_{VdW}(r) = \int_{v_1} \int_{v_2} \frac{n_1 n_2 C_6}{r^6(v_1, v_2)} d\, v_1 dv_2 \tag{2-5}$$

where $v_1$, $v_2$ represent the moveable part and the electrode, and $n_1$, $n_2$ are the densities of atoms of the two parts. Once the Van der Waals energy is calculated, the force per unit length can be computed using the following equation:

$$q_{VdW} = \frac{d(\frac{E_{VdW}}{L})}{dr} \tag{2-6}$$

For the electric field, the computation of electrostatic force is based on the calculation of capacitance of an infinitely length cylinder over an infinitely large plane, which is discussed in detail in Section 2.4. The calculation of charge distribution with this method is static, and is restricted by the geometry of the system.

If the electrostatic force and the Van der Waals force are calculated according to the geometrical design of the system, a rough result for the pull-in voltage can be acquired combined with the classic beam theory. Some of them can have analytical expression as follows. In the work by Yang and Jia [20], a linear distribution load model within the frame work of nonlocal elastic theory was proposed, without considering the charge distribution along the nanowire. For the cantilever type, the pull-in voltage can be calculated by:

$$V_{PI} = (\frac{2g^3 EI\beta_{PI}}{\varepsilon_0 \omega L^4}) \tag{2-7}$$

where $\beta_{PI}$ is the solution of $\frac{\mathrm{d}\beta}{\mathrm{d}u_T} = 0$, $\beta$ is a dimensionless quantity defined as

$$\beta = \frac{\varepsilon_0 \omega V^2 L^4}{2g^3 EI} \tag{2-8}$$

and $u_T$ is the deflection at the tip, the relationship between $\beta$ and $u_T$ is:

$$\beta = \left[\frac{120u_T}{11 - 20\alpha^2} - \frac{R_n}{(1-u_T)^n}\right] / [\frac{1}{(1-u_T)^2} + \frac{f}{1-u_T}] \tag{2-9}$$

where, $\alpha$, $R_n$, $f$ are dimensionless quantities. Ke [9] developed a nonlinear equation of nanotube-based NEMCS on continuum mechanics and nonlinear kinematics, and

gave the approximate calculation of pull-in voltage for cantilever type NEM switches, neglecting the Van der Waals effect:

$$V_{PI} \approx k_s \sqrt{1 + K_S^{FK}} \frac{H}{L^2} \ln\left(\frac{2H}{R_{ext}}\right) \sqrt{\frac{EI}{\varepsilon_0}} \tag{2-10}$$

$$k_s \approx 0.85, \qquad K_S^{FK} \approx \frac{8H^2}{9L^2} \tag{2-11}$$

The calculation process shows that the classic beam theory has the following assumptions: a continuum for the structure of the moveable part; the deflection of the moveable part is small; a static view of the electric field and the Van der Waals interaction; and geometric approximation to get the expression of the electrostatic force and Van der Waals force. When fitting the parameters, the difference between pull-in voltages recorded by the experiment and the beam theory predictions can be limited to 5% [9].

Compared to the classic beam theory calculation, molecular dynamic simulation can provide a more precise result at the nanoscale without the continuum assumption, and includes a surface effect. However, the simulation requires more time and computational resources. Comparing the results of these two methods, the MD simulation predicts a larger deflection than the beam theory [19]. As a return for huge amounts of computational work, the results from MD simulation also include stress and strain information, and can analyse the local deformation and failure problems existing in the moveable part.

In conclusion, classic beam theory can give a rough prediction about the pull-in voltage, and can fit the experiment with parameters, but many assumptions in the modelling process are improper for nanostructures from a dynamic perspective. In comparison, MD simulation provides a detailed and precise prediction of the performance of NEMCS, which can be used for further analysis about deformation, failure and many other issues.

## 2.3 MOLECULAR DYNAMIC SIMULATION

The behaviour of material at the macro-scale is based on the continuum assumption, and for some simple models the analytical solution can be obtained. All material is built up by an enormous number of molecules that are composed of atoms.

The distance between atoms is measured in Angströms ($\text{Å} = 10^{-10}\text{m}$). The continuum assumption is no longer appropriate at the nanometre ($\text{nm} = 10^{-9}\text{m}$) scale. The research objective of molecular dynamics is a group of atoms, which builds up a multibody system. It is impossible to get an analytical solution for the whole multibody problem, so the reactions between each atom should be calculated, which causes a large amount of computational work. With the help of computers, the molecular dynamic problem can be solved numerically. The first molecular dynamic research was to simulate the collisions between hundreds of hard spheres with a IBM 704 computer in the 1950s [21]. Now the development of high performance computers (HPCs) and parallel computing allows us to investigate the system with millions of atoms.

### 2.3.1 Principles of MD Simulation

The atom in the MD simulation is a hard sphere without any internal degree of freedom, so it is not suitable for studying the properties concerned with electrons and the quantum effect. Sometimes the atom model can be simplified to a point with position information and charge when studying motion. In a traditional MD simulation, the charge of the atoms is set at the beginning of the simulation and remains unchanged, and the only effect it has is the calculation of the Coulomb force. The charge transfer, neutralisation, and the polarisation effect are not included in the atom model [22].

### 2.3.2 Applications and limitations

According to *The Art of Molecular Dynamic Simulation*, MD simulation can be used to study many problems, which are listed but not limited to the following chart from the book [23].

***Table 1*** *the Applications of MD simulation* [23].

| | |
|---|---|
| Fundamental study | Molecular chaos, diffusion and transport, size effect, potential functions |
| Phase transition | First and second order, phase coexistence, order parameters, critical point |
| Collective behaviour | Decay phenomenon by time or space, vibration, spectroscopic |
| Complex fluid | Glasses, water and aqueous solutions, liquid crystal, ionic liquid |

| | |
|---|---|
| Polymer | Chains, rings, and branched molecules, equilibrium conformation, relaxation, and transport processes |
| Solid | Defect formation and migration, fracture, grain boundaries, structure transformation, radiation damage, elastic and plastic mechanical properties, friction, shock wave, molecule crystals, epitaxial growth |
| Biomolecules | Structure and dynamics of proteins, protein folding, micelles, membranes |
| Fluid dynamics | Laminar flow, boundary layers, rheology of non-Newtonian fluids |

The limitations of MD come from its principles. The model of atoms lacks the presence of electrons, so it cannot be used to study quantum phenomena. For a large system, MD simulation will take a lot of time to run and a lot of memory to store data, which restricts the number of atoms and time scale that are able to be simulated. As the empirical potential is the most important part of MD simulation, a lack of proper description of the atomic interactions can result in fatal errors in the final result.

### 2.3.3 MD model for NEMCS research

After a rough review of MD simulation, it is clear that MD has the potential to describe the working process of NEMCS, but still some barriers need to be overcome. Previous MD works on NEMCS will be presented in this section, with their findings and the gaps still remaining.

Dequesnes et al. [18] compared the MD results with linear/nonlinear beam theory, and proposed a combined method. The MD results were in good agreement with a nonlinear beam model, and the MD model could present buckling near the fixed end of the nanotube. The dynamic pull-in voltage was found to be smaller than the static pull-in voltage in the research, which highlighted the importance of developing a dynamic model for studying pull-in voltage. In their research, the electric field in MD is also calculated according to the cylinder capacitance. Fakhrabadi et al. investigated the deformation and pull-in charge of CNT-based NEMCS with different geometry and the Stone-Wales defect [5]. Their work showed that the nanotubes with large length/radius ratio and defects had a lower pull-in charge. A small number of defects could lower the pull-in charge, which resulted in a drastic drop of pull-in charge. However, the electric field in the research was described by charge, and its relation with voltage was not clear; simply fixing charge on the atom was also not accurate to describe the electric field. In their work they also discovered three-stage models of tip displacement, which will be further discussed and compared with this

work in the results part of this thesis (Chapter 5). Rasekh et al. [24] studied the dynamic response of NEMCS with a noisy input signal, and defined a pull-in voltage and pull-out voltage range. Their description of the electric field was related to the voltage using the capacitance of an infinite long cylinder, which was still not accurate and was static. Khadem et al. [25] used MD as a validation for their nonlinear model, and found that a stepped voltage could pull-in the CNT at a lower voltage.

From the work already done, the following conclusions can be drawn:

- MD simulation can provide a more detailed result including buckling and local deformation, compared with classic continuum theory;
- MD can build an NEMCS with defects and other complex inhomogeneous structures;
- The results as predicted by the dynamic equation differ from those predicted by the static equation, and it is important to use dynamic theory to study the dynamic response of the NEMCS;
- The common barrier of MD simulation for NEMCS is the setting of the electric field. Previous works applied a lot of approximations and simplifications. A more accurate description of the electric field in MD simulation is essential for future research into the dynamic response of NEMCS.

## 2.4 ELECTRIC FIELD IN NEMCS SIMULATION

This section will review the calculation approaches of the electric field adopted in previous NEMS simulations, and other methods to calculate charge distribution for utilisation in a multiphysics model as an improvement.

### 2.4.1 Charge model

For MD simulation, the simplest way to describe the electric field is to fix the charge to the atom in the system and calculate the coulomb potential:

$$E = \frac{C q_i q_j}{\epsilon r} \qquad (r < r_c) \tag{2-12}$$

where $C$ is an energy-conversion constant, and $r_c$ is the cut-off distance. The simulation with this method can only give a pull-in charge, and cannot interpret it into voltage to compare with the experimental data [10]. Setting charge on the moveable

part and electrode, and bending the moveable part, are easy, but the difficulties are in setting the amount of charge related to the voltage applied, and its distribution.

### 2.4.2 Capacitance model

Before the moveable part contacts with the electrode, the system can be treated as a capacitor. Some research used the capacitance for infinitely long metallic cylinders over and parallel to an infinitely large plain [19], [24]:

$$C = \frac{2\pi\varepsilon_0}{\operatorname{arccosh}(1+\frac{g}{R})} \tag{2-13}$$

where $g$ is the initial distance between the CNT and the electrode, $\varepsilon_0$ is the permittivity of vacuum, and $R$ is the radius of CNT. The electrostatic force per unit length is:

$$q_{elec} = \frac{d(\frac{1}{2}CV^2)}{dg} = \frac{\pi\varepsilon_0 V^2}{\sqrt{g(g+2R)}\operatorname{arccosh}^2(1+\frac{g}{r})} \tag{2-14}$$

The approximation of the electrostatic field overlooks the deformation of the moveable part, and assumes the charge is distributed evenly along the CNT since the length is infinite. But for a finite length CNT, the charge distribution is not even.

A more precise numerical model for the electric field, considering the charge distribution along the CNT, was developed based on a boundary element method (BEM) [26]. The charge distribution along the finite length CNT was simulated over an infinitely large electrode, and the result showed a great concentration at both ends of the CNT. A characteristic length $L^*$ was defined. When $L \gg L^*$, the electric field can be approximated to the combination of the infinite length (Eq. 2-14) and the concentrated charge equals to:

$$Q = CVL + Q_c \tag{2-15}$$

The concentrated charge $Q_c$ was parametrically studied. The concentrated charge reduced the pull-in voltage by 14%. The deflection was found to influence the electric field, and uniform distribution (Eq. 2-15) was acceptable when the deflection was lower than 6%. The results from this model suggested that geometric parameters and deflection could have a significant effect on the electric field, which could influence the dynamic properties of the NEMCS. Overall, this model adopted the continuum

assumption and BEM, many approximations were applied, and many parameters were fitted from the cylinder capacitance equations. Thus, there is still plenty of room for improvement.

### 2.4.3 Density function theory and atomistic moment theory

For the calculation of charge distribution along the CNT, most studies are based on density function theory (DFT). DFT results also showed a concentration of charge at the end of the CNT [27], [28]. Although DFT calculation is accurate, the calculation is a complex process, and a large system requires a lot of time and computational resources. The result of the DFT charge distribution calculation is the charge density, which needs a further step to transfer it to MD input information.

Another method for CNT charge distribution calculation is the atomistic moment theory (AMT) [29], which can provide a result similar to the DFT calculation, but the process is simpler and faster. The obtained result is the charge on each atom, which can be applied to the MD simulation directly. The calculation of the AMT is based on the following assumptions: the charge on each atom can be approximated to a point charge (which is very simular with the model of atom in MD); the potential on each atom is the sum effect of charge on other atoms and itself; the result is at the charge equilibrium state and the potential of the whole CNT is an equipotential body.

Theoretically, if the CNT has $n$ carbon atoms, the atomic interactions for atom $i$ is calculated from:

$$V_{i\sum j} = \sum_{j=1}^{n} \frac{q_j}{4\pi\varepsilon_0 |\boldsymbol{r}_i - \boldsymbol{r}_j|} \qquad (j \neq i) \tag{2-16}$$

For $n$ atoms, there are $n$ equations, which can be written as $[A]\{q\} = \{V\}$, where $\{q\}$, $\{V\}$ are the vectors for unknown charge, and set potentials. $[A]$ is an $n \times n$ matrix. The element $a_{ij}$ in $[A]$ has the following expression:

$$a_{ij} = \frac{1}{4\pi\varepsilon_0 |\boldsymbol{r}_i - \boldsymbol{r}_j|} \qquad (j \neq i) \tag{2-17}$$

When $j = i$, which presents the potential effect of the charge on their own position, and $a_{ii}$ needs further calculation. It is assumed that the charge is distributed evenly at a triangle area (according to the symmetrical structure of a hexagon), the centre of which is located at the position $\boldsymbol{r}_i$, so the voltage contribution can be calculated as:

$$V_{ii} = \iint_s \frac{q_i/s}{4\pi\varepsilon_0\sqrt{\xi^2+\eta^2}} d\xi d\eta \tag{2-18}$$

Thus, the element $a_{ii}$ is

$$a_{ii} = \frac{1}{4\pi\varepsilon_0 s}\iint_s \frac{1}{\sqrt{\xi^2+\eta^2}} d\xi d\eta \tag{2-19}$$

By solving the linear system of equations, the charge distribution vector $\{q\}$ can be obtained. The mirror image method was adopted to transfer the problem for finite length CNT over an infinitely large plain into two CNTs oppositely charged, described by a $2n \times 2n$ linear system of equations. The result was very close to the DFT result and also showed the charge concentration at the end of CNT, as **Figure 2-3** shows.

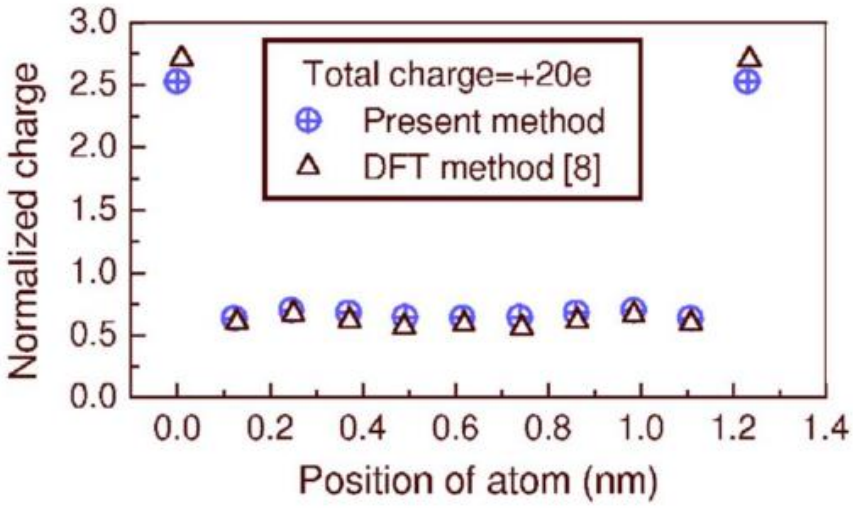


***Figure 2-3*** *The comparison between the AMT method and DFT method* [29].

From the calculation process, it can be identified that the AMT method does not have restrictions to the shape of the electrodes and the moveable parts. The result can be easily applied to MD simulation.

## 2.5 ADSORPTION ON NANO STRUCTURES

The adsorption is the phenomenon of particle adhesion to the material as a consequence of surface energy, and only happens on the surface. When the material has a large surface-to-volume ratio, the adsorption phenomenon will be significant, which is the most common case for nanostructures. The adsorbed particles will interact

with the nanostructures, and influence their physical and chemical properties. Thus, when considering the NEMCS working in a gaseous environment, the adsorption phenomenon should be included in this simulation. The adsorption can be classified as physisorption, which is caused by the Van der Waals forces, and chemisorption, which involves in the bond formation and is caused by electrostatic force. Emphasis will be put on physisorption in this review, as it is universal and more common in the NEMCS system.

### 2.5.1 Physical adsorption theory and experiment

***Pure gas adsorption***

The theoretical study of adsorption dates back to the early twentieth century. Most of the adsorption theories study the isothermal case and look for the relation of the pressure and the amount of adsorbate. According to the relation, the classic adsorption model can be classified into the following 5 types, as **Figure 2-4** shows.

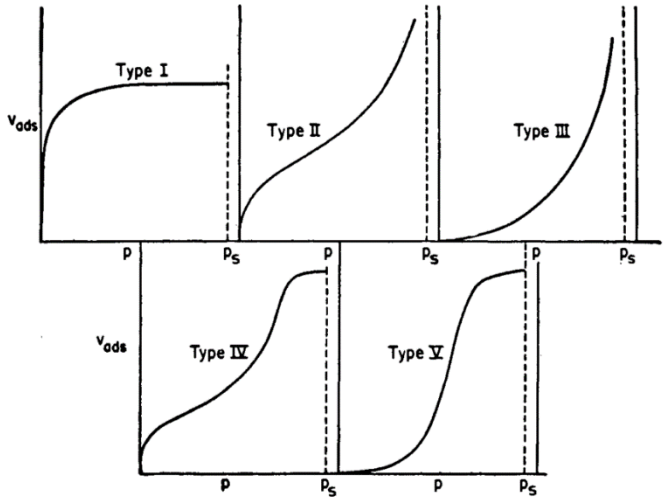


***Figure 2-4*** *The physical adsorption type according to the relation between amount and pressure* [30].

Type I is the classic Langmuir adsorption model, which describes the adsorption process as $A_g + S \leftrightarrows A_d$ like a reversible reaction, and $K = \frac{\theta}{(1-\theta)P}$, where $\theta$ is the surface coverage ratio. For low pressure, $\theta \approx KP$ and for high pressure, $\theta \approx 1$. This model assumes that only one layer of adsorbate is formed and the surface is plane and homogeneous, and suits the microporous material adsorption very well, like activated carbon. Types II and III are for nonporous material, which has strong or weak interactions with the adsorbates, and consider the formation of multilayers of adsorbate

based on the BET theory [31]. Types IV and V are for mesoporous materials and can be regarded as a combination of the multilayer and Langmuir theory. The VIth type was add to the classification in 1985; it shows a step adsorption to form multilayers, and explains the adsorption of argon or krypton on graphitised carbon blacks at below 100K temperature [32]. More specific models for these types are summarised in Foo's review paper [33].

***Mixture gas adsorption***

All the theories mentioned previously are for the pure adsorbate; however, most of the working environment of NEMCS is a gaseous mixture. Different materials show different adsorption behaviours, which is also true when gases are mixed together; therefore, trying to use one theory to summarize mixture adsorption can be misleading. One of the experimental works on $N_2$ and $O_2$ adsorption was conducted by Arnold [34] at 0°C on anatase, which showed a qualitative disagreement with the extended BET theory [35]. The liquid entropy theory he developed could only semi-quantitatively agree with the experiment. Myers et al. [36] proposed a method to calculate the gas mixture adsorption equilibria from the pure-component adsorption equilibria at the same temperature, which fitted well with the experiment and was widely used as the ideal adsorbed solution theory (IAST); but the IAST used an average inter-molecule potential to calculate the adsorption equilibria, and could not describe the selectivity in mixture adsorption [37]. So the general mixture adsorption theories are not always reliable, and are unable to give local information; so for a special case study, researchers usually apply a molecular simulation method to study the adsorption characteristics.

### 2.5.2 Adsorption simulation method

The early model for adsorption phenomenon is in a macro-experimental view, usually a combination of theoretical analysis and empirical parameters. Now molecular simulation methods enable scientists to look at the adsorption phenomenon in a micro-way, and analyse the problem locally at the nanoscale. The major difference between the macro-theory and molecule simulation for adsorption is that molecule simulation can show the fluctuations on the adsorption amount and the instantaneous local concentration of the adsorbate, which can be translated into the property fluctuations and their confidence intervals in nano-structures and nano structure-based devices. In this section, the molecule simulations on the gas adsorptions on nano

structures will be reviewed, and the appropriate method for the NEMCS multiphysical model will be described.

***Grand canonical Monte Carlo method***

The most common method for adsorption simulation is the grand canonical method (GCMC), which uses the Monte Carlo method in the grand canonical ensemble. The grand canonical ensemble (or $\mu, V, T$ ensemble) describes a system in open contact with a reservoir, and is close to the adsorption case, by performing a series of insertions and deletions of the adsorbate gas molecules. In the ensemble, the chemical potential $\mu$ and the temperature are fixed, and the equilibrium status is that the adsorbate molecules have the same chemical potential and temperature in the reservoir.

Arora et al. [38] used the GCMC method to simulate adsorption inside the single wall carbon nanotube (SWCNT). In their simulation, the SWCNT and the gas molecules are fixed rigid. They found that the inside nitrogen molecules can form multiple adsorption layers inside a large diameter SWCNT under high pressure. Based on the adsorption structures, a double Langmuir was used to fit the adsorption amount, which is consistent with the GCMC result. Wang et al. [39] simulated hydrogen adsorption in SWCNT for potential storage use. They adopted a combined method of a multiple-timestep path integral hybrid Monte Carlo method with GCMC [40], which is more precise for quantum fluids. They studied the hydrogen adsorption on SWCNT arrays, individual SWCNT, and carbon slit pores, and found that the carbon slit pores have better hydrogen storage ability.

***Canonical Monte Carlo method***

Another MC method for adsorption simulation is to use a canonical ensemble. Rafati et al. [41] used a canonical Monte Carlo method to study the adsorption of pure oxygen, nitrogen, and mixtures on SWCNT under different pressures and temperatures. But the sum of nitrogen adsorption on the inside and outside surfaces they provided is much less than the inside adsorption amount of the GCMC result [38] under the same conditions and SWCNT diameter. This was caused by the misinterpretation of pressure. In GCMC, the pressure and temperature of gaseous reservoir are translated into chemical potential, and the system was controlled by the chemical potential with insertions and deletions of gas molecules, which means that moving another gas molecule into the system requires the same energy as moving

another into the gaseous reservoir without CNT. For CMC, the system is controlled by temperature. The number of gas molecules remains the same throughout the whole simulation, and the pressure is calculated by an equation of status (EOS) for every case. This way of interpreting pressure is acceptable without adsorption. When the system has a significant adsorption phenomenon, the pressure will decrease, which is lower than the result calculated from the EOS, and overestimation of the system pressure results in the underestimation of the system adsorption. Since the difference is caused by misinterpretation of the overestimation of the system pressure, the trend of the results and comparison between their cases are still referable. Rafati found out that oxygen has a better adsorption than nitrogen on SWCNT [41]. In their results, they didn't discuss the adsorption changes with the percentages of the nitrogen and oxygen in mixture. It was not pointed out, but could be found out in their work, that the adsorption amount increases with increased oxygen percentage, by comparing the adsorption amount at 313K for equimolar $O_2$ and $N_2$ with the air composition.

***Molecular dynamic simulation***

Another method for adsorption simulation uses MD simulation. The MD simulation has the same problem as the CMC method in interpreting pressure. Another problem for MD is that when the system is large and complex, and the temperature is low, it will take several minutes or even hours to reach the equilibrium status in reality. For MD, usually the timestep is in femoseconds, and that will require a huge amount of computational work. But one advantage for MD simulation is that diffusion properties can be studied at the same time. Cheng et al. [42] used MD simulation to study the hydrogen adsorption in SWCNT of different diameters and chiralities. In their work, they took curvature into consideration, by using Lennard-Jones potential parameters with $sp^2$ and $sp^3$ hybridisation empirically:

$$\sigma(r) = f(r)\sigma_{sp^2} + [1 - f(r)]\sigma_{sp^3} \tag{2-20}$$

$$\epsilon(\mathrm{r}) = \begin{cases} f(r)\epsilon_{sp^2} + [1 - f(r)]\epsilon_{sp^3}^{exo} & exohedral \\ f(r)\epsilon_{sp^2} + [1 - f(r)]\epsilon_{sp^3}^{end} & endohedarl \end{cases} \tag{2-21}$$

where $f(r) = (1 - r_0/r)^{\lambda}$, $r_0 = 1.356\text{Å}$ is the radius of (2,2) nanotube, assumed to have purely $sp^3$ bonding. The parameters used in the simulation are from ab initial calculation. They found that the adsorption amount is mainly dependent on the diameter, and chirality has little effect. The adsorption energy of the armchair structure

is slightly larger than the zigzag structure. They also found that the diffusion of hydrogen in CNT is much larger than for microporous materials like zeolite.

***Density function theory***

Density function theory (DFT) can also be used in adsorption simulation, especially for simple geometry structures, like slits and cylinders. It is difficult to apply DFT to a complex system, like zeolites [43]. DFT can provide a convincing result not only for physisorption, but also chemisorption, which is beyond the applications of MC or MD simulation. Using DFT, Han et al. [44] investigated hydrogen physisorption and chemisorption in SWCNT, and calculated the energy barrier is about 78.837 kcal/mol to transform from physisorption to chemisorption for hydrogen. They only studied the adsorption on the SWCNT outside surface, and considered the closed-ended carbon nanotube.

Summarising the methods for adsorption simulation, except for presenting the structure of the adsorption layer and the adsorption amount, every method has its own advantages: the GCMC method can have a solid interpretation of pressure, so its results are comparable with experiments under the same pressure; MD simulation can give the structure of adsorption layer as well as the diffusion properties of the adsorbate; DFT can provide a precise result and can be used for chemisorption study. For adsorption in NEMCS operating in atmosphere, chemisorption can be neglected, and the diffusion properties are not relevant, so GCMC simulation is an ideal method to simulate the gaseous environment. Different from the adsorption of nanostructures in previous work, when the moveable part and the electrode are charged, the gas molecules in the environment will polarise, and there will be electrical attractions between the gas molecules and NEMCS, so the adsorption amount will be larger than that that caused by the Van de Waals force.

## 2.6 VIBRATION TEST FOR NANO STRUCTURES

### 2.6.1 Vibration in NEMCS and its influence

Although the pull-in process of NEMCS does not involve vibration motion, in the pull-out process, the moveable part will not go back to the initial position directly. After the voltage is reset, the moveable part will have an initial displacement, and it will vibrate around the balance position with damping. Since previous studies on NEMCS are focused on the pull-in voltage, how the vibration in the pull-out process

affects the performance of NEMCS is not thoroughly investigated. When the next signal is applied and the moveable part is still vibrating, caused by the previous signal, the feedback of NECMS will be different. A lower voltage can pull-in the movable part, which can generate a misleading result according to the initial settings of the system. The response of NEMCS is more complex than the linear time invariant (LTI) system, and the output signal is not the convolution of the input signal and the response function. The NEMCS system is a nonlinear time-dependent system which is presented in **Figure 2-5**. When the input signal is larger than the pull-in voltage, the output will be nonzero after a period of response time; otherwise it remains zero, which is nonlinear. When the next signal is close to the previous one, and the moveable part is still vibrating at large amplitude, there will be a nonzero signal in the output, even though the voltage is lower than the pull-in voltage, so the system is time variant. The response time of the second input will be shorter, since displacement has already occurred and the output value will have a linear relation with the previous one if the resistance is not changed.

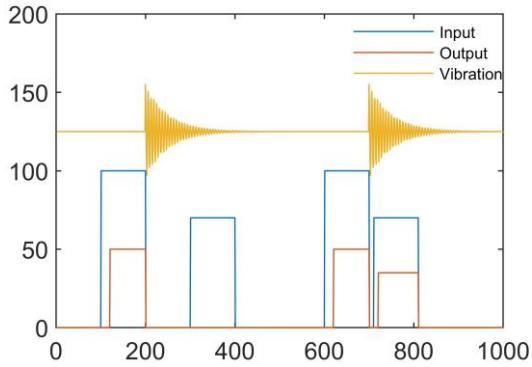


***Figure 2-5*** *The nonlinear time-dependent feature of NEMCS.*

Since the NEMCS system is a time-dependent system, vibration properties are important in the NEMCS working mechanism. More specifically, the damping of the moveable part has a dominant effect on the working frequency capability of NEMCS. In the following, studies on the vibration of nano structures will be reviewed. Although the pull-out process is not thoroughly discussed in NEMCS work, the vibration of nano structures has been investigated by many researchers, and their results can be applied to NEMCS study.

***Damping***

Damping can be caused by intrinsic factors and the external environment. The intrinsic cause of damping has been studied by thermal elastic damping, surface damping, defect damping and quantum effect damping.

The thermoelastic damping model is developed on the base of an anelastic model, which adds the first time derivatives of stress $\sigma$ and strain $\epsilon$ on the base of Hooke's law, and has the following expression:

$$\sigma + \tau_\epsilon \dot{\sigma} = M_R(\epsilon + \tau_\sigma \dot{\epsilon}) \tag{2-22}$$

where $\tau_\epsilon$ is the stress relaxation time while strain is kept at a constant, and $\tau_\sigma$ is the strain relaxation time while stress is a constant. $M_R$ is the elastic modulus after relaxation. When the stress and strain is changing periodically, the elastic modulus is a complex value which depends on the vibration frequency. The quality factor $Q$ can be approximate to the ratio of the imaginary part and real part of the elastic modulus, when the quality factor is small, and can be calculated by

$$Q_T^{-1} = \Delta_M \frac{\omega\tau}{1 + (\omega\tau)^2} \tag{2-23}$$

where $= \sqrt{\tau_\epsilon \tau_\sigma}$ , and $\Delta_M$ is the relaxed strength of the modulus. For the thermoelastic solid, the relaxation strength can be calculated as: $\Delta_E = \frac{E_{ad} - E}{E} = \frac{E\alpha^2 T_0}{C_p}$, where $\alpha$ is the thermal expansion coefficient, and $C_p$ is the heat capacity. Following these theories, Zener calculated the quality factor as $Q_z^{-1} = \frac{E\alpha^2 T_0}{C_p} \frac{\omega\tau_z}{1+(\omega\tau_z)^2}$ , where $\tau_z = \frac{b^2}{\pi^2 \chi}$ , $b$ is the width of the beam, and $\chi$ is the thermal diffusivity of the solid [45]. Lifshitz et al. [46] presented another way to estimate quality factors for thin rectangular beams as $Q_L^{-1} = \frac{E\alpha^2 T_0}{C_p}\left(\frac{6}{\xi^2} - \frac{6}{\xi^3}\frac{sinh\xi + sin\xi}{cosh\xi + cos\xi}\right)$, where $\xi = b\sqrt{\frac{\omega_0}{2\chi}}$. Since these analytical calculations were based on the assumption of rectangular thin long beams, directly using them for CNT vibration quality factors could generate errors.

Another source of damping is the surface effect, which increases with the surface to volume ratio, especially for the nanostructures. However, the analysis of the surface damping is mostly based on the defects on the surface instead of on surface tension [47]. Assuming that the elastic modulus of the surface is different from the bulk one, the surface elastic modulus was represented by $E_s$, and the depth of the surface range

is $\delta$. The calculation for the surface damping with the two elastic modulus is as follows:

$$Q_s^{-1} = \frac{2\delta(3w+t)}{wt}\frac{E_s}{E} \tag{2-24}$$

where $w$ is the width and $t$ is the thickness of the beam. Although this result is calculated theoretically, the $E_s$ and $\delta$ are derived from experimental measurements.

Besides the defects on the surface, inside defects will influence the quality factor of the beam differently. Czaplewski et al. [48] used a Debye-like equation to calculate the dissipation caused by internal defect:

$$Q_D^{-1} = A\frac{\omega\tau_D}{1+(\omega\tau_D)^2} \tag{2-25}$$

where $A$ is the parameter describing defect density, $\tau_D$ is the relaxation time of the defect, and follows the Arrhenius relation with temperature $\tau_D^{-1} = \tau_{D0}^{-1}\exp(-\frac{E}{k_B T})$.

With the scaling of the devices and lowering of the temperature, the quantum effect should be taken into consideration, since in a classical view, the atom will be limited within an energy well, but in quantum mechanics, the atom can tunnel through the energy barrier. Anderson et al. [49] described glasses with a Two Level System (TLS) model, which now becomes a standard tunnelling model. The damping caused by the quantum effect can be calculated by [50]

$$Q_{TLS}^{-1} = \frac{\pi}{96}C_{l,t}(\frac{T}{T_{co}})^3 \qquad (T \ll T_{co}) \tag{2-26}$$

$$Q_{TLS}^{-1} = \frac{\pi}{2}C_{l,t} \qquad (T \gg T_{co}) \tag{2-27}$$

where $C_{l,t}$ is the tunnelling strength and $T_{co}$ is the temperature where the relaxation rate equals the angular frequency. A comparison between the relaxation time rate and strain frequency shows whether the system can reach the thermal equilibrium status. Ahn et al. [51] spotted the phonon pumping mechanism for internal quantum friction, which also used the two-level model for defect. At zero temperature, the quality factor had the following relation:

$$Q_{pp}^{-1} \propto \frac{1}{\omega\tau_\epsilon^*}\frac{n\gamma^2}{\rho v^2} \qquad (T=0) \tag{2-28}$$

Except for internal damping, the dissipation of mechanical energy can be caused by external forces. Two major sources are from the clamped end and the environment, and for NEMS, circuit dissipation should also be considered.

The clamped end dissipation is caused by the concentration of stress at the clamped end, and the mechanical energy will be transferred into the support structure, which is more significant for a beam without the axial load applied, since the stress concentration at the clamped end is more obvious. Cross et al. [52] investigated the vibration loss at the abrupt junction, and found $Q_C^{-1} \propto \frac{v_g}{l\omega} T_n$, where $v_g$ is the group velocity of the wave, and $T_n$ is the energy transmission coefficient of the mode n at frequency $\omega$. For a two-dimensional model of a cantilever, the in-plane quality factor is $Q_{in-plane}^{-1} \propto (\frac{\omega}{l})^3$, and $Q_{out-plane}^{-1} \propto \frac{\omega}{l}$. Based on the 2D in-plane model, Hao et al. [53] compared the junction dissipation for a cantilever and double clamped beam. They found that the cantilever had less clamping dissipation than the double clamped beam.

In the vibration system, the damping caused by thermal motion, defects, surface, and clamping conditions are coupled together, and it is difficult to validate the theory through separate experiments. The surrounding environment damping can be separated easily by changing the environment. For theoretical analysis, the description of the gas or liquid in the environment can be divided into two extreme conditions. One is the interactions between the molecules (ignored for the approximation of low pressure gaseous environment); the other is the continuum model for the modelling of the liquid environment and gaseous environment at high pressure. In the first model, damping is caused by the collision between the gas molecules and the beam, and the quality factor can be calculated by $Q_g^{-1} = (\frac{2}{\pi})^{\frac{2}{3}} \frac{1}{\rho t f_0} \frac{P}{v}$, where $t$ is the thickness, $P$ is the pressure, and $v$ is the velocity of gas molecule [54]. For the second model, the force on the vibration from the liquid environment is described by viscosity, and the quality factor can be approximated by $Q_l^{-1} = \frac{3.8\mu}{\sqrt{E\rho}\omega} (\frac{L}{t})^2$, where $\mu$ is the viscosity of the liquid. Another cause of damping by the environment is squeeze-film damping, which is caused by the gas or liquid between the moveable part and the substrate, and has the following relations with geometry: $Q_{sf}^{-1} = \frac{\mu}{4\sqrt{E\rho}\omega} (\frac{L}{t})^2 (\frac{\omega}{g})^3$ [55].

In summary, damping in the NEMCS system can be caused by multiple sources. Many models have been built to describe different kinds of damping with assumptions and simplifications to get a final analytical result. For intrinsic damping, the models are mostly developed based on the thin beam theory, and using the result directly for tube-like structure damping is questionable.

***Beat***

When two sine waves vibrate together, their combined amplitude can be transformed using the algebraic function:

$$\cos(2\pi f_1 t) + \cos(2\pi f_2 t) = 2\cos\left(2\pi\frac{f_1 + f_2}{2}t\right)\cos\left(2\pi\frac{f_1 - f_2}{2}t\right) \qquad (2\text{-}29)$$

When the two frequencies are close, the total amplitude will change periodically, and this is called the beat phenomenon. The beat frequency is the double frequency of the second term regardless of the phase, which is $f_{beat} = |f_1 - f_2|$.

The beat phenomenon can appear in more complex vibration systems than the two-dimensional homogenous beam. When the beam is not symmetrical in shape or homogenous for the material, the vibration frequency in different directions will have slight differences, which satisfies the condition of the beat phenomenon. As when the beam has inside damage, the free vibration will show the beat phenomenon, which can be used for damage detection [56]. Also, the beat can be caused by damping. Yalla et al. observed the beat phenomenon in a combined structure-liquid damper [57]. In forced vibration, if the frequency of excitation is near resonance, the beat phenomenon can also be observed [58]. In summary, for vibration without periodic excitation, the cause of the beat is either intrinsically the asymmetry of the structure, or externally the damping of the environment. For vibration with periodic excitation, certain frequencies of excitation can result in the beat phenomenon.

For NEMCS working in atmosphere, the damping from the environment and the beat phenomenon caused by the local asymmetry adsorption can appear in this complex system.

### 2.6.2 Vibration of Nanostructures by Experiment

Most vibration experiments of nanostructures can be categorised into two groups according to the purpose of research. For a new nanomaterial, usually the vibration test is one way to get the mechanical properties, like the elastic modulus of the

material, which is easier than doing a tensile test at nanoscale. The setup for these experiments is simple vibration for a cantilever or double clamped beam structure. The other group uses vibration of the material with knowledge of mechanical properties to design devices like NEMCS, resonators, sensors etc. Usually the vibration experiments in this group have a more complex structure or environment. Damping and the beat phenomenon can appear in these experiments, and influence the actual performance of nanostructures.

Since the vibration test in experiments usually needs the help of SEM and a transmission electron microscope (TEM) to visualise the outcome of the vibration test, the experimental work on nanostructures' vibration is mostly done in vacuum to get a clear image. The conclusions from a vacuum experiment can have limitations when applied to the second group of experiments, since the working environment of the device is no longer a vacuum. When scientists want to study the vibration in a non-vacuum environment, AFM is a usual choice of visualisation tool to set up the experimental work. In this sub-section, the experimental work on nanostructures' vibration both in a vacuum and a fluid environment will be reviewed to see the intrinsic properties and the environmental influence.

***Vibration experiment in vacuum***

As previously suggested, vibration can be used to get the mechanical properties of nano structures. At nanoscale, vibration can be caused by the thermal motion without manual excitation. Basing on the thermal vibration amplitude of CNT under TEM, Treacy et al. [59] estimated the Young's modulus of CNT to be in the terapascal range, using the following equations:

$$W_n = \frac{1}{2} c_n u_n^2 \tag{2-30}$$

$$c_n = \frac{\pi \beta_n^4 Y (a^4 - b^4)}{16 L^3} \tag{2-31}$$

where $W_n$ is the vibration energy and $\langle W_n \rangle = kT$, $u_n$ is the vibration amplitude, $Y$ is the Young's modulus, $L$ is the length of CNT. The undamped vibration frequency is:

$$\omega_n = \frac{\beta_n^2}{2L^2} \sqrt{\frac{Y(a^2 + b^2)}{\rho}} \tag{2-32}$$

The nano structures can also vibrate with the excitation of external force. Poncharal et al. [60] used electric force to drive the vibration of CNT, and they found out that the amplitude of the vibration changed with the frequency, which was consistent with the damped harmonic vibration. They also found that the resonance frequency did not shift with the increase of amplitude, which indicated that the vibration would remain linear for large amplitude deflection; however, in their article, the largest amplitude they tested is not clarified, so this conclusion is questionable. Their result for Young's modulus could also reach 1 TPa for small diameter CNT, but the Young's modulus dropped to 0.1 TPa when the diameter increased to 40 nm. The vibration could also be excited by AFM tips [61], and this method can be used to test non-conductive nanostructures like polymer nanotubes.

The damping phenomenon has been observed and studied in vacuum experiments. Eichler et al. [62] studied the damping of mechanical resonators made from CNT and graphene, and found that damping largely depended on the vibration amplitude. So they added the nonlinear term $\eta x^2 dx/dt$ to the motions of equations. Since the damping was no longer linear, they derived a new way for calculating the quality factor by $Q = 2\pi E/\Delta E$, which satisfied $Q = 1.09 f_0/\Delta f$, and the result was very close to the linear damping effect. For the origin of the damping, they suggested contamination and geometrical nonlinearity, and pointed out that the effect of frictions, clamping configurations, and suspended length should be studied in future work. The highest quality factor they got is 100,000 for a graphene resonator, which was at 90 mK, close to absolute zero point. They also took tensile stress conditions into account for the damping phenomenon, and got a similar result.

Except for the stress condition, there are lots of factors which can influence the damping phenomenon in nanostructures' vibration. Carr et al. [63] investigated the damping phenomenon in silicon wires' vibration, and found a dependence on surface to volume ratio. They tested two groups of silicon nanowires with a thickness of 100 nm and 200 nm and different widths, and found out that with an increase of surface to volume ratio, the quality factor dropped. Olkhovets et al. [64] investigated the damping of single and double clamped Si beam vibration under different temperatures, and found that the internal energy dissipation had a peak value in the $T = 160 \sim 190K$ range. They explained the mechanism by Debye relaxation $Q^{-1} \propto \frac{\omega\tau}{1+(\omega\tau)^2}$ , $\tau =$

$\tau_0 \exp(\frac{E}{k_B T})$. The damping peak will shift to a higher temperature with a frequency increase, which was also consistent with their experiment. In another work [65], by lowering the temperature, they also observed an increase of vibration frequency. For ultralow temperatures, Zolfagharkhani et al. [66] investigated the damping at millikelvin temperature, and fitted their result with the following relation: $Q^{-1} \propto T^{0.36}$, which fits the data at a temperature higher than 0.1 K, but gave a large difference for the data at temperatures lower than 0.1 K. For other factors, Yang et al. [67] optically actuated the 170 nm thick silicon cantilever, and found that the reduction of oxygen groups of the surface can improve the quality factor of the resonator. Yang et al. [68] investigated over the surface treatment effect on the quality factor, and concluded that: for a cantilever with a length shorter than $30\mu m$, clamp dissipation was the dominant effect; for a longer beam, the geometry and the surface effect were the dominant effects; this was a very subjective conclusion from the experimental results. They also found that heat treatment can improve the quality factor of a silicon nanowire by removing the $SiO_2$ and adsorbate layer.

Since the silicon nanowires are made by lithography, it is easy to investigate the relationship between damping and other factors with a series of samples by changing the geometry. However, for CNT, collecting samples with the expected geometry can sometimes be difficult. With the development of CNT fabrication techniques, scientists can finally investigate systematically the damping of CNT vibration. The results of these two materials are comparable and share many things in common. Compared with the silicon nanowire, the quality factor of CNT was generally lower with similar geometry parameters [69], which could be explained by the surface effect on the damping phenomenon, since CNT had a larger surface to volume ratio. The quality factor of CNT could be improved by lowering the temperature: when the temperature was lowered to 20 K the quality factor could increase up to 2000 [70]. When the temperature dropped to 20 mK and tensile stress was applied, the frequency could reach above 350 MHz, and the quality factor could reach up to $10^5$ [71]. With the lowering of the temperature, the quality factor increased linearly with $T^{-0.36}$, which is the same as for the silicon nanowire [71], [66].

***Vibration experiment in fluid environment***

Liu et al. [72] excited silicon nanowires by impulse signals at room temperature and pressure; the frequency they got was in the gigahertz range, and the quality factor was 18. They also observed that the quality factor was related to the geometry of a silicon nanowire, but they did not give explanations. The innovation of their work is that they analysed the vibration signal in the time domain, and showed that the vibration amplitude after the excitation was affected by the phase when the excitation stopped, which could be controlled by the excitation time. Although they calculated the quality factor in the frequency domain, they analysed the signal in the time domain, and their results made a significant contribution to NEMS-based computation and information storage.

The CNT vibration tests in a gaseous environment mainly used the CNT whose diameters were around 1 nm, which were much less than the mean free path of the atmosphere. Garcia-Sanchez et al. [73] used scanning force microscopy to study the CNT resonator vibrating in air. The highest frequency they got was 3.1 GHz for the 265 nm long MWCNT clamped at both ends. The quality factors varied from 3 to 20. The low quality factors could be caused by the scanning tip and the gaseous environment. The increasing of the scanning interaction didn't change the quality factors, so gas damping should be the dominant factor. By comparing their result with beam theory, they found that the beam theory fitted the MWCNT very well, but produced a difference for the SWCNT vibration. The frequency of SWCNT vibration in the experiment is larger than the beam theory's prediction, and they explained this by tension, slack and contamination.

Sazonova et al. [74] investigated the damping caused by air in a CNT oscillator from the pressure of 10 torr to vacuum, and found that the quality factor decreased from 40 to 10 when the pressure increased. Their result agreed with the theoretical calculation [75]. In another work, CNT vibration was reported to reach the frequency of gigahertz at room temperature and pressure, and the estimated Young's modulus was 80 GPa [76].

### 2.6.3 Vibration simulation

***Vibration simulation in vacuum***

Jiang et al. [77] used molecular dynamic simulation to investigate the damping of CNT oscillator with a many-body Brenner potential and found the quality factor obeyed the law of $T^{-0.36}$ from 0.05K to 293K, which broadened the $T^{-0.36}$ law range. Compared with the experimental result of silicon nanowire [64], the damping peak at around 160K did not appear. Vsllsbhaneni et al. [78] used molecular dynamic simulation to study SWCNT cantilever vibration with adaptive intermolecular reactive empirical bond order (AIREBO) potential, to describe the carbon-carbon interaction. They investigated the geometry parameters, chirality, and temperature effect on the frequency and damping of vibration in the axial and transverse directions. The quality factor $Q_t$ in the transverse direction was affected by length ($Q_t \propto L^{\theta}, 0.8 < \theta < 1.4$), and diameter $D$ ($Q_t \propto D^{\mu}, 1.4 < \mu < 1.6$), and for a nanotube with similar diameter, chirality had limited effect on the quality factors. In addition, the axial quality factor was not influenced by either these geometry parameters or chirality. For the influence of the temperature, they took the quantum effect into consideration, and modified the temperature below Debye temperature. Damping in two directions was affected by temperature in the relation of $Q \propto T^{-\alpha}$, with $\alpha > 1$ below Debye temperature and $\alpha = 1$ above Debye temperature, which showed a large difference from previous $T^{-0.36}$ relations. To explain their result, they used classic thermoelastic dissipation theory and phonon-phonon damping theory, but there still remained a difference.

***Vibration simulation in fluid***

For fluid damping in nanowire vibration, the continuum assumption and Stokes drag calculation are no longer suitable, since the geometry parameters of a nanowire are smaller than the mean free path, and a high frequency causes unsteady effects. Bhiladvala et al. [75] used collision theory to calculate the damping coefficient for the case where the beam size was smaller than the gas mean free path. For the case when the gas mean free path was smaller than the beam size, and the continuous assumption was reasonable, they used an unsteady solution for the surrounding fluid to take the high frequency effect into consideration. Their results suggested that compared with the microscale beam, the nanowire had a higher quality factor when vibrating in an atmosphere of room temperature and pressure.

Hutcherson et al. used MD simulation to investigate the air damping for microbeam operated at low pressures in one dimension near a fixed wall [79]. They found that the damping mostly depended on the frequency, and when the frequency was less than 3 MHz, their relation was almost linear. The oscillation amplitude had ignorable influence on damping when it was small. Li et al. extended Hutcherson's work to torsional plate and flexible beam investigation [80].

Chen at al. investigated the nanoscale fluid-structure interaction between water and CNT, using MD simulation [81]. They found out that at a high speed, the Stokes law failed to give a fine prediction for flow resistance, because of the reduction of viscosity due to local heating. Later, they studied the viscous damping on nano beam resonators, surrounded by water vapour [7]. Some overdamped cases were observed at high water vapour concentration. However, most of their work concentrated on developing an analytical expression on damping using classic theory, which had little difference with bulk material. The setup of their MD simulation was simple, and the influence of temperature, pressure, and adsorption were not considered.

Sawano et al. also investigated the CNT cantilever resonators in water by experiment, and used MD simulation to test the size limits of continuum theory[82] . They suggested that the no vortex motion was in the system, and the continuum theory for vibration and viscous fluid were applicable. Interestingly in their experiment, the fundamental oscillation disappeared and the second oscillation remained.

In conclusion, several MD simulations on vibration properties in fluid have been conducted. However, the settings for the fluid environment were either at extreme low pressure, or extreme high density. The adsorption effect has not been considered in their models.

## 2.7 SUMMARY AND IMPLICATIONS

From the literature, it can be found that although the classic beam theory is well established, while applying it to the nano structures, significant errors will arise due to neglecting surface effects. An atomic-scale model was developed for the NEMCS simulation. However, the previous models did not include a proper electric field calculation. According to literature, AMT method can give a close result to the DFT electric field calculation, as such AMT will be adopted to combine with the MD to establish a more realistic model for NEMCS.

The fluid field at the nanoscale also deviates from the classic theory prediction, and the adsorption at the nanoscale induces significant influences. Unfortunately, there is no literature talking about the adsorption influence on vibration. Thus, the GCMC method will be utilized to simulate the adsorption and combine it with MD simulation to probe the performance of NEMCS in a more realistic manner.

# Chapter 3: Research Design

Reviews of previous work in this field report that, although many simulations of multiphysics modelling of the NEMCS have been conducted, the simulation method for the electric field can be improved by considering deformation and geometric restrictions. Also, how CNT-based NEMCS works in a gaseous environment is still unclear. This chapter will introduce the design of the research and the methods adopted in building the multiphysics model of the CNT-based NEMCS device. Section 3.1 presents the adsorption simulation method; Section 3.2 shows the simulation process of vibration on the basis of adsorption simulation results; Section 3.3 introduces a separate study on the electric field simulation method; and Section 3.3 gives the details of parameters for setting up each system.

## 3.1 SIMULATION METHOD FOR ADSORPTION

GCMC simulation is applied to simulate the adsorption phenomenon on CNT. Pure $C_{12}$ (10, 10) SWCNT with a length of 173.24 Å (41 structure periods in the CNT axial direction) is considered, which is open-ended. The CNT is fixed at both ends. Nitrogen and oxygen are selected for the adsorption simulation as they are the major components of air. The bond potential within the diatomic gas is described by the harmonic bond and is given by: $E_{bond} = K(r - r_0)^2$, where $r_0$ is the equilibrium bond length and $K$ is the bond coefficient. The settings for each coefficient are listed in **Table 2**.

***Table 2*** *The bond coefficient for different gases.*

| **Bond type** | $\boldsymbol{K}$ $(\frac{\boldsymbol{ev}}{\text{Å}^{\boldsymbol{2}}})$ | $\boldsymbol{r_0}$ (Å) |
|---|---|---|
| N-N[38] | 71.6 | 1.10 |
| O-O[83] | 20.7 | 1.208 |

GCMC simulation relies on a series of insertions and deletions of the adsorbate molecules at random positions in the system, calculating the amount of change of total energy, and comparing it with the settings for chemical potential. The gas molecules are rigid during the GCMC simulation, and the bonding coefficients actually come into

effect in later vibration simulations. Usually the chemical potential is calculated by the sum of ideal chemical potential $\mu^{id}$ and excess chemical potential $\mu^{ex}$. The excess chemical potential is zero for the fictitious gaseous reservoir, and is non-zero for the interacting system. The ideal chemical potential is calculated from:

$$\mu^{id} = kTln\frac{P\Lambda^3}{kT} \tag{3-1}$$

$$\Lambda = \sqrt{\frac{h^2}{2\pi mkT}} \tag{3-2}$$

where $k$ is Boltzmann's constant, $T$ is the temperature, $P$ is the pressure, $\Lambda$ is the thermal de Broglie wavelength, $h$ is the Planck's constant, and $m$ is the mass of the gas molecule. For the chemical potentials of mixed gases, the chemical potential is set by the partial pressure of each component. It is notable that GCMC simulation is a dynamic process, and as such the absorption amount should fluctuate with the simulation time (but with a constant time average).

## 3.2 SIMULATION METHOD FOR VIBRATION IN A GASEOUS ENVIRONMENT

### 3.2.1 MD simulation settings

The vibration simulations use the results of an adsorption model, and are carried out in three scenarios: the complete scenario, with adsorption on both inside and outside surfaces of CNT; the partial scenario, with only outside surface adsorption; and the partial scenario, with only inside surface adsorption. The system, as obtained from GCMC simulation, is first relaxed for 250 ps in a NVT ensemble (where atom number N, system volume V, and temperature T is fixed) at the corresponding temperature. The excitation is applied to the CNT and the adsorbed gas. The CNT is clamped at both ends, and the excitation velocity has a distribution of sine function along its axis: $v(z) = \lambda sin(kz)$. The value of $\lambda$ should be large enough to make the damping phenomenon observable in the background of thermal noise, and as small as possible to limit the nonlinear component in vibration. The excitation is applied in four directions, as illustrated in **Figure 3-1**, and should have different vibration results due to the adsorption-induced asymmetry. The vibration simulation is conducted under NVE ensemble (where atom number N, system volume V, and total energy E is fixed). During the relaxation and vibration, a virtual wall is applied at the CNT ends in the

last two partial adsorption scenarios to avoid inside gas molecules going out or outside molecules coming in. The interactions between the walls and gas molecules are defined by the LJ potential.

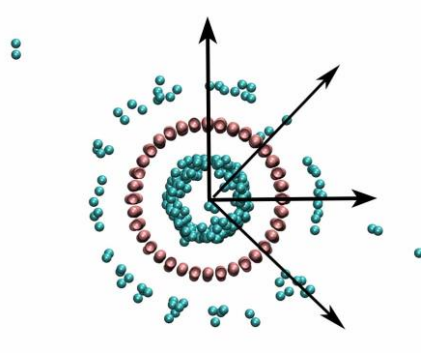

***Figure 3-1*** *The excitation directions in the vibration test*

### 3.2.2 Vibration properties calculation method

The displacement of the CNT centre is tracked to get the vibration signal. Frequency and time are the two key aspects for analysis of a vibration signal. Fourier transform is used to transform the results from the time domain into the frequency domain to get the natural frequency. But the result of Fourier transform does not include the frequency change information according to time. To investigate the frequency change in the adsorption-vibration model, short-time Fourier transform (STFT) is adopted, which divides the whole time into several parts, and does the Fourier transform calculation separately.

Apart from frequency, damping is another important property in the adsorption-vibration model. There are several parameters which can be used to describe damping, including: quality factors $Q$ and damping ratio $\zeta$. Measurement of these two parameters can be made from the frequency domain and the time domain.

In time domain, the most common method to calculate damping ratio is logarithmic decrement method (LDM). For a system with viscous damping with an impulse excitation, the amplitude response $y$ has the following expressions with time:

$$y(t) = y_0 \exp(-\zeta \omega_n t) sin \omega_d t \tag{3-3}$$

where $\omega_d$ is the damped natural frequency, and $\omega_d = \sqrt{1-\zeta^2}\omega_n$. The decay of peak amplitude $A$ after $r$ cycles can be calculated by:

$$\frac{A_{i+r}}{A_i} = \exp[-\frac{\zeta}{\sqrt{1-\zeta^2}} 2\pi r] \quad (3\text{-}4)$$

so the logarithmic decrement is: $\delta = \frac{1}{r}\ln\left(\frac{A_i}{A_{i+r}}\right) = \frac{2\pi\zeta}{\sqrt{1-\zeta^2}}$ . When $\zeta < 0.1$ , the following approximation can be used:

$$\zeta = \frac{\delta}{2\pi} \quad (3\text{-}5)$$

The damping parameters can also be calculated in the frequency domain, using the bandwidth method. The quality factor $Q$ is defined as the ratio of natural frequency $\omega_n$ and the half-power bandwidth $\Delta\omega$ , and their relationship with $\zeta$ can be simplified as follows, when $\zeta < 0.1$:

$$Q = \frac{\omega_n}{\Delta\omega} = \frac{1}{2\zeta} \quad (3\text{-}6)$$

In the adsorption-vibration model, since the frequency of the system shifts with time, calculating the damping ratio in the frequency domain can give a larger result than damping in reality. In this research, the damping ratio is calculated with LDM in the time domain, to avoid the influence of the frequency shift.

## 3.3 SIMULATION METHOD FOR ELECTRIC FIELD

The AMT method will be adopted to calculate the electric field. As discussed in Section 2.4.3, it gives a precise result comparable with that obtained from DFT calculations. It also gives a more precise description than the charge model and the capacity model when the CNT and graphene electrode are deformed. To model the NEMCS, a cantilevered CNT is chosen as the moveable part and one layer of graphene is taken as the gate and drain electrode. To describe the atomic interactions within the system, the adaptive intermolecular reactive empirical bond-order (AIREBO) potential [84] was used to describe the atomic interactions between carbon atoms within the CNT and graphene. The interactions between the CNT and graphene include the electrostatic interactions and Van der Waals (VdW) interactions. The VdW interaction is described by the 12-6 LJ potential, with a cut-off distance of 10 Å. The system is firstly minimised using a conjugate method and then relaxed under 300K using an NVT ensemble for 5 ps. A small timestep of 0.5 fs is chosen, since the coulombic force

is usually much larger than the VdW force in the NEMCS system. The equilibrated system is used to calculate the initial charge distribution.

According to the AMT, the electric potential of each carbon atom on CNT is set to 30 V, and carbon atoms on the graphene to 0 V to build an electric potential difference of 30 V, which should be large enough to pull in NEMCS, according to the experimental work [2] and the calculation from Eq. (2-10). The potential is set three times larger than the prediction by Eq. (2-10), to make sure the charge distribution has an obvious and quantifiable difference. Then a linear system of equations can be built as:

$$[A]\begin{Bmatrix} q_{CNT} \\ q_{gra} \end{Bmatrix} = \begin{Bmatrix} U \\ 0 \end{Bmatrix} \tag{3-7}$$

where [$A$] is the matrix the element of which is the potential coefficient from each atom to the specific atom position. The detailed calculation method for [$A$] is introduced in Section 2.4.3. $\{q_{CNT}\}$, and $\{q_{gra}\}$ are the unknown vectors for the charge distribution on each atom of the CNT and graphene respectively. $\{U\}$ is the potential vector for the CNT, and $\{0\}$ is the potential vector for the graphene, corresponding to $\{q_{CNT}\}$ and $\{q_{gra}\}$. By solving this equation system, the charge on each atom can be acquired, which is then assigned to each corresponding atom for the electric field simulation. Since the bending of the CNT will influence the charge distribution, the charge distribution should be updated with the position of atoms during the MD simulation. As such, AMT is coupled with MD simulation to update the atom charge at a given frequency, as schematically shown in **Figure 3-2**. Presumably, the charge distribution will be more accurate if the update frequency is sufficiently high.

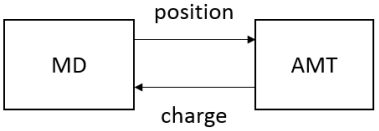


***Figure 3-2*** *Loop for dynamic electric field simulation*

This method cannot be used for the piezoelectric material calculation, since the potential created by strain is not considered. Also, both (5,5) CNT and graphene are not reported to have such piezoelectric properties. It is assumed that the CNT and graphene are isopotential bodies during the charge distribution update.

## 3.4 THE SYSTEM SET UP DETAILS

For the adsorption simulation, a (10, 10) SWCNT with a length of 173.24 Å is chosen. The SWCNT and the gas molecules are put into a cuboid simulation box. The SWCNT is in the middle of the simulation box and in each direction the edge atom has a 20 Å distance to each box surface to eliminate the boundary influence. The periodic boundary condition is applied to the system. Different gaseous environment simulations are considered, including pure nitrogen, pure oxygen, and the gas mixture of nitrogen and oxygen with different partial pressures. Adsorption of different gaseous environments is simulated at 100 K under room pressure. A low temperature is chosen to produce a large adsorption amount, and a large difference in adsorption amount in different gaseous environments, which can make a noticeable difference to vibration properties in vibration simulations. For the pure nitrogen case, the temperature is chosen to be from 100 K to 400 K to investigate the temperature influence. For the pressure case study in a pure nitrogen environment, the temperature is set to 100 K. Different pressure values ranging from zero to two bars are considered. The vibration simulations start with the result of adsorption simulation, and use the same settings for potential and boundary conditions.

For the dynamic electric field simulation, the moveable part is a $(5,5)$ SWCNT, and the length is 88.04 Å (21 structure periods in axial direction); the electrode is a single layer of graphene sheet with a width of 100.84 Å, and the length is 24.14 Å; the gap between the CNT centre and the graphene sheet is 20 Å. A cuboid simulation box with a non-periodic shrink-wrap boundary condition is used. The minimum distance between each simulation box surface and the NEMCS system is 20 Å. The temperature is set to 300 K, and the voltage is 30 V. Different update frequencies of the charge distribution were examined.

Since these two studies are isolate with each other, different CNTs have been chosen. In the adsorption vibration study, a larger CNT was chosen to make sure the difference between adsorption amounts in different cases are detectable. In the electric field study, a smaller CNT was chosen to reduce the computation cost. Both methods have no restrictions, and can be applied to all kinds of CNTs.

For MD and GCMC simulation, the open-sourced Large-scale Atomic/Molecular Massively Parallel Simulator (LAMMPS) is employed. The AMT calculation for the electric field is realised through MATLAB. The visualisation is

conducted by Visual Molecular Dynamics (VMD). All simulations are carried out on the high-performance computer (HPC) service provided by the Queensland University of Technology.

# Chapter 4: Vibration in Gaseous Environment

In this chapter, the influence of the gaseous environment on the resonance properties of NEMCs will be investigated. Section 4.1 will first discuss the gas adsorption, and the adsorption structure will be analysed in Section 4.2. The vibration properties under a gaseous environment will be discussed in Section 4.3.

## 4.1 GAS ADSORPTION SIMULATION RESULT

For the GCMC gas adsorption, the basic model for the adsorbent is a (10,10) single wall CNT, and the length is 173.24 Å, which is larger and longer than the model in the electrical field simulation, to make sure that the adsorption phenomenon is significant and less influenced by local thermal fluctuations. The adsorption is simulated on the inside and outside surface of the CNT. During the first GCMC simulation, the number of atoms first increases and then fluctuates around a certain value (as shown in **Figure 4-1**).

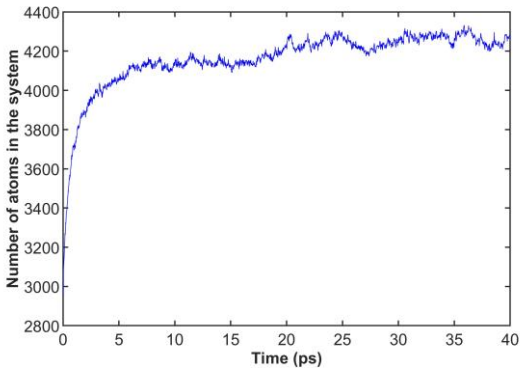


***Figure 4-1*** *The number of atoms during the first GCMC simulation (for $N_2$ adsorption at 100 K and 0.5 bar).*

A second GCMC simulation follows to eliminate the error caused by some pre-calculated values, as the system density increases in the GCMC simulation process. The atom number in the second GCMC is fluctuating (as shown in **Figure 4-2**).

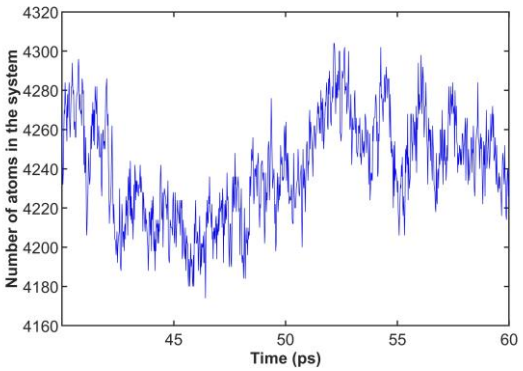


***Figure 4-2*** *Atom number fluctuating in the second GCMC simulation (for $N_2$ adsorption at 100 K and 0.5 bar).*

In the isothermal investigation for $N_2$ adsorption at 100 K, the adsorption amount increases with pressure (shown in **Figure 4-3a**). The fluctuation of gas number is around 200 atoms, which is the same at all pressures. The value of the final timestep is marked out instead of the average value, because the value of the final time step is what can be used for vibration simulation instead of the average value. Although the average value can eliminate the error caused by thermal fluctuation, it lacks detailed information of molecule positions and cannot be used for later vibration simulation. Using the final timestep value can also show the growing trend of the adsorption amount with pressure.

In the isobaric investigation of $N_2$ adsorption at 1 bar, the adsorption amount drops fast with an increase in temperature (as shown in **Figure 4-3b**). Although the number of gas molecules in the system drops very fast when the temperature increases, at 300K, there are still 50 molecules in the system. According to the equation of status of an ideal gas, without considering the adsorption phenomenon, there would be around 15 molecules in the same simulation box (defined in Section 3.4) and under the same pressure and temperature. It is apparent that even at room temperature, the adsorption phenomenon is still very significant.

$N_2$-$O_2$ mixture adsorption simulation is also performed to investigate whether or not the NEMCS will be sensitive to the gas components. In the gas mixture adsorption investigation at 100 K and 1 bar, pure $O_2$ has the maximum adsorption amount and the next is pure $N_2$ (shown in **Figure 4-3c**), which is consistent with previous CMC simulation result [41]. The gas mixture has a lower adsorption amount than the pure gas. With the increase of $N_2$ percentage, the total adsorption amount increases. The

results for mixture adsorption are difficult to explain directly, and will be discussed in Section 4.2.

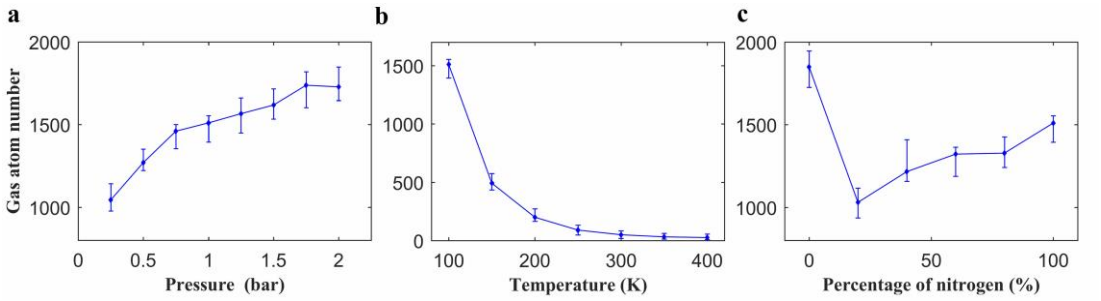


***Figure 4-3 (a)*** *The isothermal $N_2$ adsorption curve at 100K;* ***(b)*** *the isobaric $N_2$ adsorption curve at 1 bar;* ***(c)*** *the $N_2$ and $O_2$ mixture adsorption amount at 100K 1bar. The error bars present the maximum and minimum number of gas atoms in the second GCMC simulation and the marker point is the gas atom number at the final timestep.*

For the adsorption result on the final timestep, the gas atoms on the inside and outside surface of the CNT are counted separately, which can be helpful for later explanations of the vibration and damping behaviour. Since the final timestep of 2 bars gives a false interpretation of the trend in the total isothermal curve, it is not included in the region adsorption analysis. Likewise with the pure $O_2$ adsorption result, which is discussed later. The inside and outside adsorptions follow the same trend with the total adsorption amount, but at different rates (shown in **Figure 4-4a**). For the isothermal curves, the outside molecule number under the 1.75 bar is almost twice than that of the 0.25 bar. In comparison, the inside molecule number only shows an increase of ~ 20%.

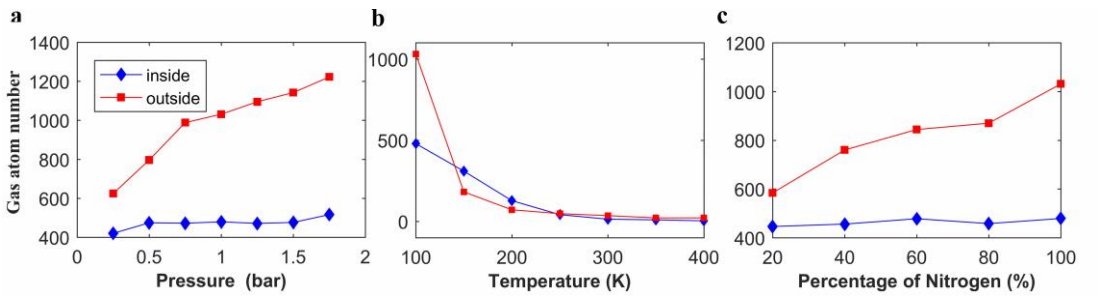


***Figure 4-4*** *The adsorption result for inside and outside region of CNT.* ***(a)*** *the isothermal curve for $N_2$ at 100K;* ***(b)*** *the isobaric curve for $N_2$ at 1 bar;* ***(c)*** *the $N_2$-$O_2$ mixture adsorption amount at 100K 1 bar.*

In the isobaric curves, the outside gas number drops faster than the inside below 150 K, but drops slower when the temperature is higher, which leads to a higher outside adsorption amount between 150 K and 250 K (shown in **Figure 4-4b**). From the geometric perspective, the outside surface has a larger adsorption radius and should have a larger adsorption amount for the same material. The results reveal the fact that the adsorption amount is more than a surface area issue in the nanotube system, and the inside adsorption amount can be larger than the outside; the cause will be analysed in following section. For the mixture adsorption amount, the outside adsorption shows a more sensitive change to $N_2$ than the inside adsorption (shown in **Figure 4-4c**). The outside adsorption amount shows more than 60% increase when the percentage of $N_2$ increases from 20% to 100%, while the inside doesn't show a significant increase in atom number.

Summarising the GCMC adsorption simulation result, the adsorption amount changes with pressure, temperature, and the percentage of $N_2$ in the mixture, and the changing rate is different for inside adsorption and outside adsorption. Some features in the results need further explanation and discussion, as follows.

## 4.2 ADSORPTION STRUCTURE ANALYSIS

The isothermal curves of inside adsorption and outside adsorption are different in shape. By checking the adsorption configurations visualised by VMD (shown in **Figure 4-5**), it can be seen that the inner region has formed a two layered adsorption structure, but there is only one adsorption layer on the outside surface, which explains why the adsorption on different surface has different isothermal curve. For the outside adsorption, only one adsorption layer is formed, so the isothermal curve should be like a typical Langmuir adsorption model from 0.25 bar to 2 bar [30], For the inside adsorption, bilayer adsorption configuration has been found, so the isothermal curve at this pressure range should be like a combination of Langmuir theory and multilayer adsorption model. The bilayer adsorption model can explain why the inside adsorption increases at 0.25~0.5 bar, and 1.5~1.75 bar, while the amount remains almost the same between 0.5~1.5 bar (shown in **Figure 4-4a**). The first adsorption layer forms at lower pressure and saturates at around 0.5 bar. The second adsorption layer only forms at higher pressure than 1.5 bar, which brings the increase from 1.5~1.75 bar.

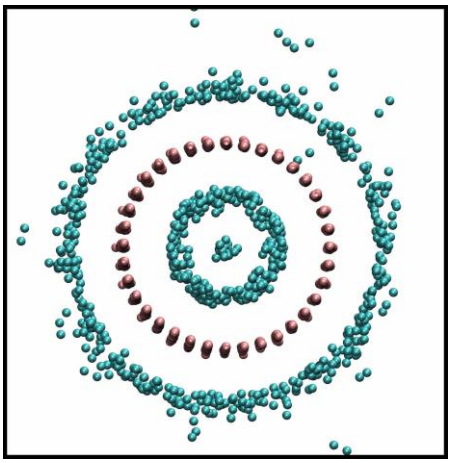

***Figure 4-5*** *The adsorption configuration at 0.5 bar 100 K. The inner region has formed a two layered adsorption structure, but there is only one adsorption layer on the outside surface. (The black wire frame shows the boundary of the figure and is not the actual size of simulation box. Same for following figures)*

Arora et al. [38] have used GCMC to simulate the zigzag CNT (n,0) inside adsorption, and observed the two-layered adsorption for CNTs with large diameter as well (larger than (15, 0) CNT), which can be explained by Brunauer-Emmett-Teller (BET) theory [31], where the second adsorption layer is the adsorption layer of the first layer. Compared with their results, the current simulation for $N_2$ adsorption on (10, 10) CNT at 100K 1 bar is slightly larger than that of the (17, 0) CNT (shown in **Figure 4-6**). Since the radius of the (10, 10) CNT is 14.1Å, i.e., slightly larger than the (17, 0) CNT (about 13.3Å), this observation indicates that the current results agree well with previous work on inside adsorption. Since Arora et al. investigated the adsorption in a large pressure range (from $10^{-6}$ to $10^{2}$ bar) with sparse data points, while in current research, the pressure varies from 0.25 to 2 bar, there is limited data which can be referred to. As the current trend and one simulation case is consistent with previous work, current results are reliable, and the deletion method can give a similar result with the GCMC moves in specific region. As for the adsorption configuration, previous work also shows the formation of a bilayered adsorbate structure, so the formation of such two layered adsorbate structure is irrelevant with the chirality of CNT.

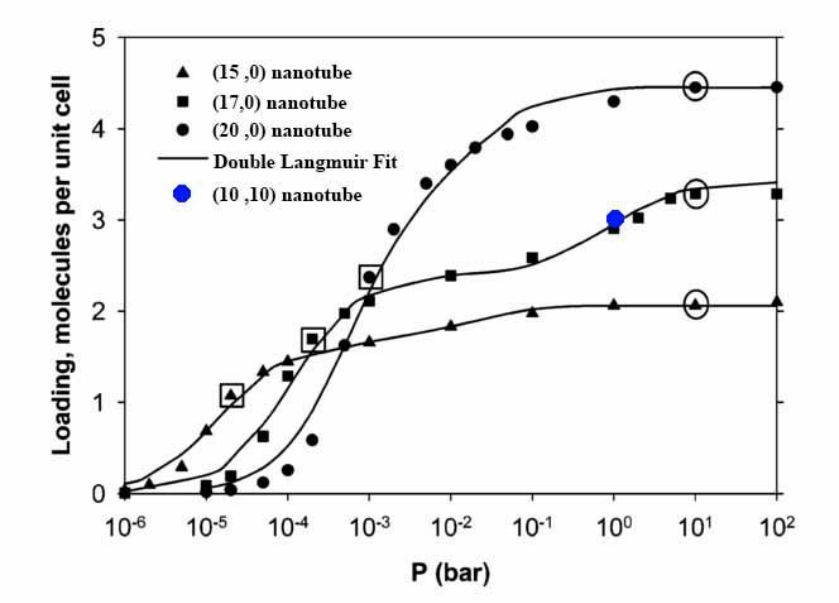


***Figure 4-6*** *Comparison with Arora's work* [38]. *Only the blue dot is the result from current simulation. Current result is similar for CNT with similar diameter, regardless of chirality.*

As for the isobaric curve, no previous study was found in the literature. As mentioned previously, the inside adsorption amount is larger than the outside from 150K to 250K (shown in **Figure 4-4b**), although the adsorption radius is smaller for the inside region, and the potentials between the $N_2$ and the inside surface and outside surface are set at equal. From a classic adsorption theory viewpoint, in the same conditions, a larger adsorption radius means a larger adsorption area, and more adsorbate can be fit into the adsorption area, which fits the results at 100K and above 250K. However, the results contradict the classic theory at 150K to 250K. Some speculations can be used to explain such a contradiction: firstly, the bilayer structure is only observed for the inside gas molecules, and the second layer makes the inside adsorption amount larger than the outside; secondly, the inside gas molecules are trapped inside the tube once adsorbed in it, and are not likely to escape if the temperature is low, but the outside gas molecules don't have such problem; thirdly, the adsorption phase of inside gas changes slower in that temperature range than the outside, and different adsorption phases make the adsorption amount incomparable in certain temperature ranges.

The first speculation is direct and easy to test. The adsorption configurations at 150K, 200K, and 250K are visualised with VMD. The bilayer adsorbate doesn't appear

above 150K (shown in **Figure 4-7**), so the first speculation is not correct. From the adsorption at 100K, it can be observed that the molecule number in the second layer is quite small and the sum of the two layers is still smaller than the outside adsorption amount. In the adsorption configuration at 150 K, the inside gas molecules are close to others, which is similar with that at100 K, but the outside gas molecules are not so close to each other. At 200 K, a clear whole adsorption ring inside the CNT can be spotted, but the outside ring is already broken. Until the temperature reaches up to more than 250K, the inside gas molecules are not tight together, and show a similar phase with the outside gas molecules. According to the atomic configuration, the third speculation does exist. The second speculation is a dynamic explanation and cannot be proved by the static adsorption configuration figure.

Once the gas molecules enter into the CNT, a lot of energy is required for them to escape. The inside region of a CNT is an almost closed region and the only exits are the two ends. For the outside gas molecules, the energy required to leave the adsorption layer is much smaller. Specifically, the kinetic energy that dominates the adsorption phenomenon is determined by temperature. At temperatures between 150~250K, the kinetic energy is large enough for the outside gas molecules to leave the adsorption layer, but not enough for the inside molecules to get out, so more gas molecules are trapped inside the CNT, causing a larger adsorption amount. The simulation results prove that the adsorption cannot be treated as a pure problem of geometry area, for the CNT-like structure with an almost sealed space and a small entrance for gas. The kinetic energy of adsorbate should also be taken into consideration.

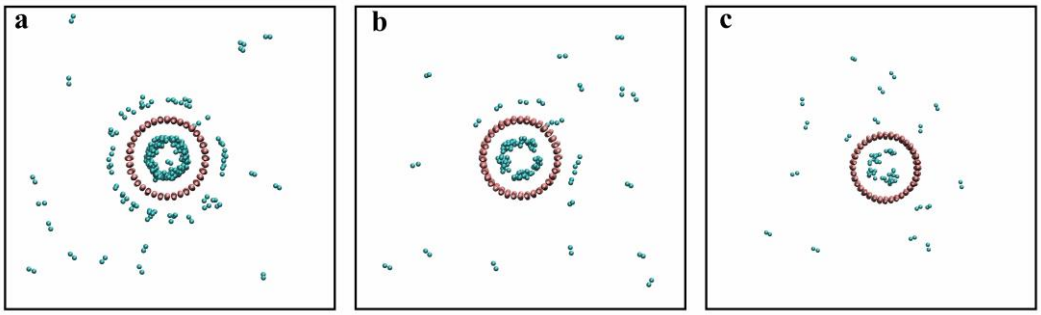


***Figure 4-7*** *The adsorption configuration at* ***(a)*** *150 K;* ***(b)*** *200 K; and* ***(c)*** *250 K.*

For the mixture adsorption, it is found that the mixture adsorption amount is lower than each of the pure components. Meanwhile, pure $O_2$ has a higher adsorption amount than pure $N_2$, but the mixture adsorption amount increases when the $N_2$

percentage increases. Similar results are also reported in the literature. For instance, the CMC results [41] gave a mixture adsorption amount between the adsorption amounts of pure components at 313K; another GCMC method combined with the ab initial simulation gave the mixture adsorption amount as lower than for each component [37]. For the actual experiment [34], the mixture adsorption amount was slightly lower than for the pure componenta. As for the adsorption amount relation with percentage, the CMC result suggested that the adsorption amount was increasing with the $O_2$ percentage at 313K, which is different from the current finding at 100K.

As aforementioned in the Literature Review (Section 2.5), there is no universal rule to determine the mixture adsorption amount according to the pure component. The interactions between adsorbate components and between adsorbate and adsorbent vary in different cases, which will eventually influence the final mixture adsorption amount. In this study, the curve is explainable from the LJ potential coefficient. Although the depth of well $\epsilon$ of C-O pairs is greater than N-O pairs, the zero potential distance $\sigma$ of C-O is larger than N-O, which means the minimum energy distance $r_m \approx 1.122\sigma$ is larger. Thus the average adsorption distance of oxygen is longer than nitrogen, and this is proved by the adsorption configuration (shown in **Figure 4-8**). Since the nitrogen molecules are closer to the carbon nanotube surface, the nitrogen adsorption layer can affect the oxygen adsorption. Oxygen can be hard to adsorb on the CNT surface and the mixture adsorption amount is determined by the nitrogen. That is why the adsorbed molecule number increases with the increase of nitrogen percentage. However, when the nitrogen molecules in the mixture are few, this influence should be weakened. To test this, the percentage of nitrogen is set to 1% and the adsorption amount is close to pure oxygen, which is more than the adsorption amount of pure nitrogen.

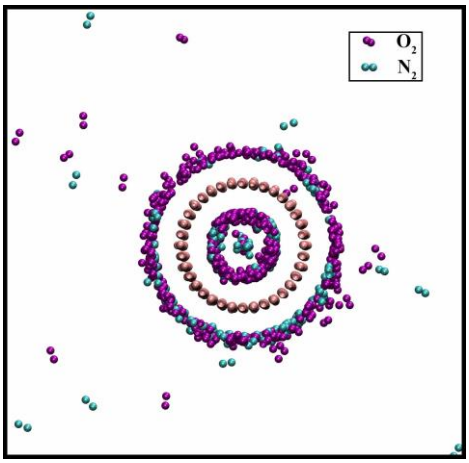


***Figure 4-8*** *The $N_2$-$O_2$ mixture adsorption configuration in the axial direction view.*

It is worthwhile to discuss how reliable the simulation method is in interpreting the mixture adsorption phenomenon. Although the mixture chemical potential is the sum of each component's chemical potential according to partial pressure, for each component in the mixture, the chemical potential should be equal to the chemical potential of the mixture. In GCMC moves, the average energy difference for inserting or deleting a molecule is based on the total potential, rather than the partial potential. Therefore, during the GCMC simulation, no matter what percentage of $N_2$ is in the atmosphere, the potential settings for $N_2$ and $O_2$ can only be the potential of the mixture, and the percentage of $N_2$ cannot be set. In other words, current GCMC simulation doesn't actually have the ability to do the mixture adsorption at certain percentages. To realise the simulation of mixture adsorption at certain percentages for the component, current GCMC simulation should be further improved. To illustrate, another simulation was carried out where the $N_2$ and $O_2$ chemical potentials were set by the mixture's chemical potential. The modified GCMC result also shows a smaller adsorption amount for the mixture (shown in **Figure 4-9**).

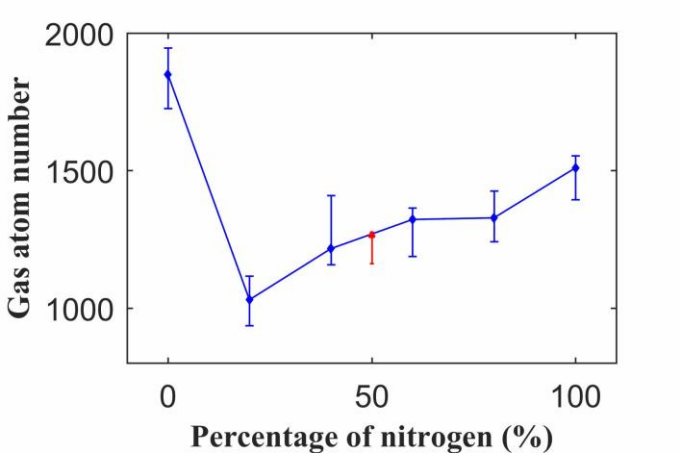


***Figure 4-9*** *The modified GCMC result compared with previous results. The red point is the modified adsorption amount, and is put at 50% because the GCMC setting parameters for nitrogen and oxygen are the same.*

Although mixture adsorption simulation still has some issues, it can still be used for the further vibration test to see the influence of adsorption on damping, since the configuration of adsorption is reasonable and the bilayer adsorption structure exists inside the tube. Although the vibration result of a mixture cannot be related to a certain pressure, it can still be used to draw some conclusions regarding the adsorption amount, and investigate whether NEMCS vibration is sensitive to gas type in the environment.

## 4.3 VIBRATION SIMULATION RESULT AND DISCUSSION

Vibration tests for each adsorption are carried out in four directions (shown in **Figure 3-1**) based on the adsorption model, with the CNT in vacuum as a reference. A small velocity excitation is given to the nanotube and adsorbed gas, which is smaller than the adsorbed energy of $N_2$ (0.11eV [85]). During the simulation, the adsorbed gas molecules move with the CNT, which are not influenced significantly by the vibration (the loss of adsorption amount is less than 3%). By tracking the motion of the mass centre (based on the middle unit of CNT) in the excitation direction, the vibration and damping characteristics can be obtained. The damping caused by gas is more significant than that caused by the CNT structure and clamped ends (shown in **Figure 4-10**). For vibration in a gaseous environment, after the obvious damping in amplitude, there is a rise of the amplitude and then a drop (shown in **Figure 4-10b**). In the damping process, the seventh peak is higher than the previous peak (highlighted in red

circle). The process is not purely damping but has the increase of amplitude. This characteristic is not unique and exists in most cases. When the damping ratio is low, it is more obvious and steady (shown in **Figure 4-10c**). For the same case, different random seeds can change the results. It can be simply identified as noise caused by the gas, or such noise can be explained by the asymmetry of the system and the beat phenomenon.

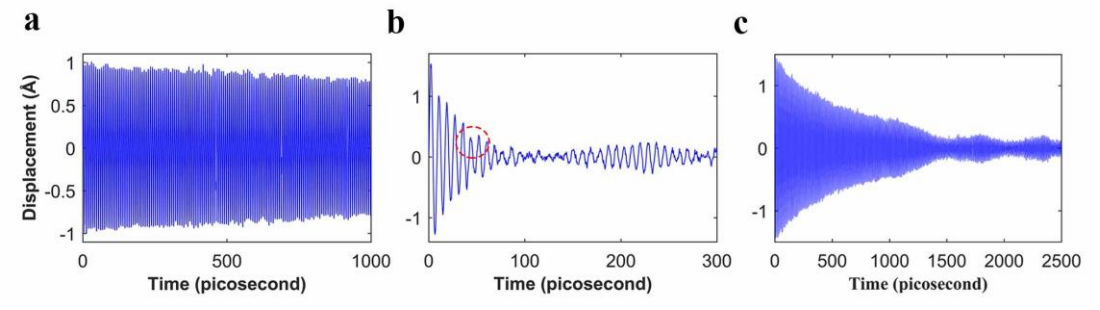


***Figure 4-10*** *The time-displacement curve for vibration* ***(a)*** *in vacuum;* ***(b)*** *in 0.75 bar $N_2$ at 100 K;* ***(c)*** *damping caused by inside adsorption $N_2$ at 0.5 bar, 100 K.*

### 4.3.1 Influence of gas in the vibration model

***Beat phenomenon***

The pure CNT without adsorption has a symmetrical structure, and during the vibration, it has only one frequency. However, in a gaseous environment, the CNT adsorbs gas molecules at random positions and the structure becomes asymmetric. When such an asymmetrical structure vibrates, it will have different frequencies in different directions. Since such differences are caused by the adsorbed gas molecules, the frequency change will be small. According to previous studies and theory [86], two close frequencies vibrating together will cause the beat phenomenon, which can happen in two different transverse directions of one nanostructure [86]. So the asymmetric adsorption-vibration model is likely to have the beat phenomenon.

To measure the asymmetry of the system, the mass centre distribution in different directions is plotted using the following method. Since the CNT has deformation during the simulation process, the reference point (origin point) needs to be re-centred. The CNT is broken into 41 sections in an axial direction. The mass centre of each section is calculated and set as the origin, and each section is divided into 36 regions in the cross-section area. The relevant positions of the regions' mass centre to the origin are calculated. The relevant positions in the same region but

different sections are later averaged to show an overall mass centre distribution (shown in **Figure 4-11**).

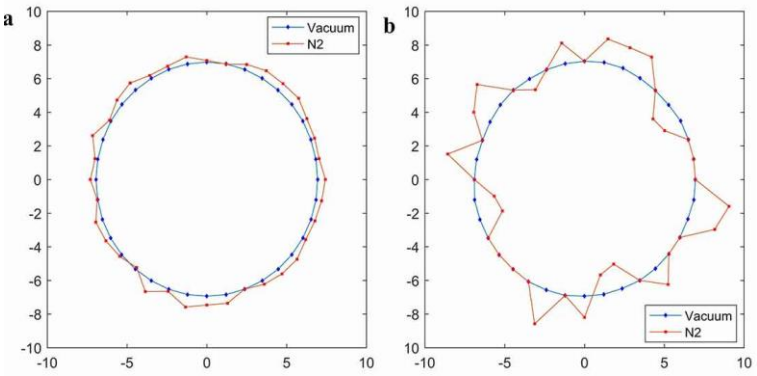


***Figure 4-11*** *Mass centre distribution in different angle regions from* ***(a)*** *the whole length,* ***(b)*** *the middle section.*

A pure CNT has a symmetrical mass centre distribution in vacuum, but the CNT with $N_2$ absorption is highly asymmetrical. Such asymmetry is a local property. Comparing the mass centre distribution in the whole length and that in the middle section, the asymmetry in the middle section is more significant than in the whole length. In the whole length, the local difference brought by random adsorption is eliminated by averaging while calculating the mass centre.

To prove that the asymmetrical distribution of mass centres can result in the beat phenomenon, two models are built up for vibration test. One is the CNT with $C_{14}$ replacing the original $C_{12}$ randomly, called structure A. The other is the CNT with extra $C_{12}$ attached at random sites on CNT (mimicking a surface modification effect), called structure B (shown in **Figure 4-12**). The first model is for the asymmetrical mass distribution in different directions, while the mass centre distribution is symmetrical, and the second model is for asymmetrical mass centre distribution in different directions.

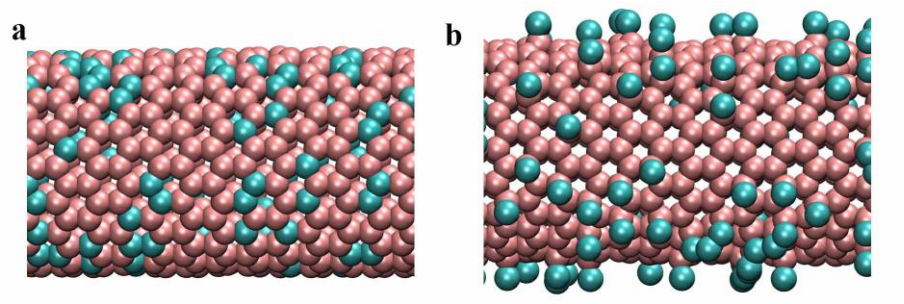


***Figure 4-12*** *The CNT derivative structures of* ***(a)*** *A model with random* $C_{14}$ *and* ***(b)*** *B model with random* $C_{12}$ *attaches.*

For structure A, the vibration has a single frequency (shown in **Figure 4-13a, b**). For structure B, a clear beat phenomenon can be seen in the displacement figure, and two close but separate peaks show up in the FFT result (shown in **Figure 4-13c, d**). Besides, structure B has an obvious damping trend in the displacement figure, which also causes a wider band gap in the FFT result than for structure A. These results suggest that asymmetrical mass distribution caused by isotopes cannot induce the beat phenomenon, and the damping effect is marginal. However, surface modifications will significantly alter the vibrational behaviours of CNT and result in a large damping effect.

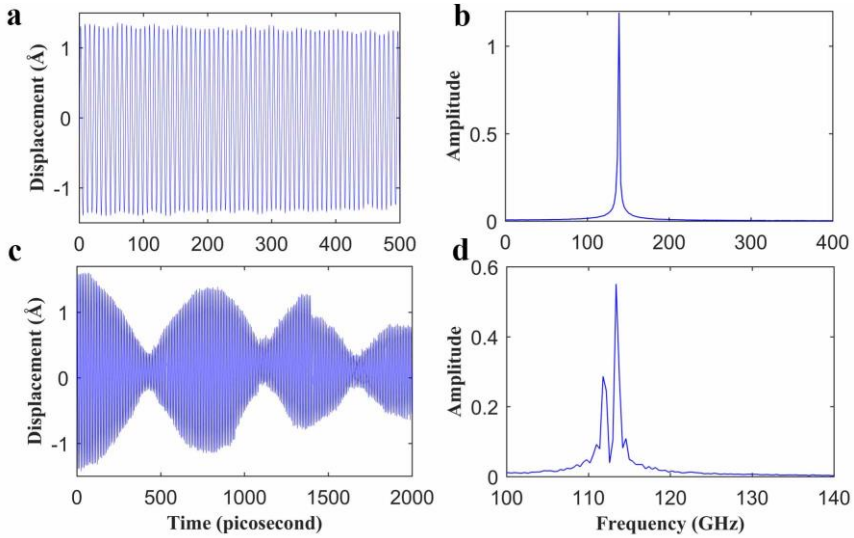


***Figure 4-13*** *The displacement curve for structure A* ***(a)*** *and B* ***(c)*** *and their FFT results* ***(b)*** *and* ***(d)***.

To investigate how the distribution of surface modifications will affect the beat period, more samples have been tested, by keeping a constant amount of surface atoms, but using different random distributions. The distribution of surface modifications exerts profound effects on the vibrational behaviours of CNTs, in terms of the vibration amplitude, damping, and natural frequency (shown in **Figure 4-14**).

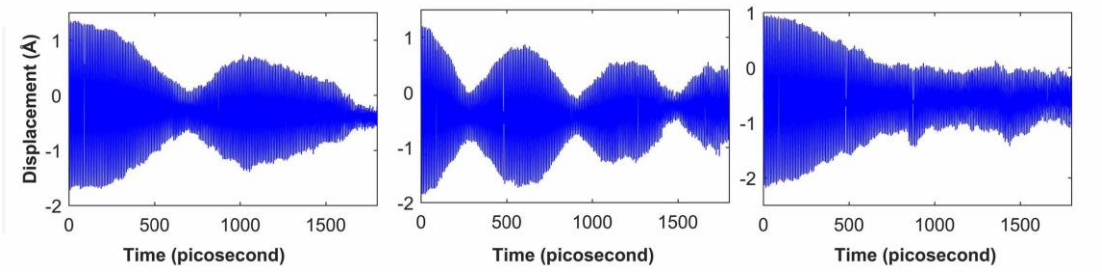


***Figure 4-14*** *Different time-displacement curves for structure B with different randomly attached sites.*

Reconsidering the gas adsorption vibration model, the adsorbed gas molecules can change the mass centre distribution and cause a beat phenomenon similar to those observed in structure B. Since the interaction between the gas molecule and the CNT is not as strong as the carbon-carbon interaction, and the relevant positions of gas molecules on the CNT as well as the adsorbed amount are always changing, such factors will induce a changing effect on the vibrational behaviours of CNTs.

***Shift of frequency***

Another phenomenon caused by the motions of the gas molecules is the shift of vibration frequency of the CNT. The frequency of the system is always changing during the simulation. Instead of a clear sharp peak in the FFT result for pure CNT, the FFT results for adsorbed CNT are quite noisy and the main peaks are built by many small peaks close to the main frequency as shown in **Figure 4-15a**. Since FFT does not include time information, it cannot present the frequency shift during the simulation. In this regard, the short time Fourier transform (STFT) algorithm is adopted, which divides the time into eight parts, and does FFT separately for each part. As shown in **Figure 4-15b**, the main frequency has a small shift with time. Thus, using the FFT result to calculate the damping ratio is not accurate, since the bandwidth is not only caused by damping, but also by the frequency change. It is more reasonable to use time domain information for damping ratio calculation. However, although the logarithmic decrement method (LMD) calculates the damping ratio in the time domain,

it also assumes the frequency remains unchanged, but provides a damping ratio smaller than the FFT results. Thus, a more accurate damping ratio computation method for the vibration with changing frequency needs to be developed, which is beyond this research topic. Here the LDM method in the time domain is used as a compromise.

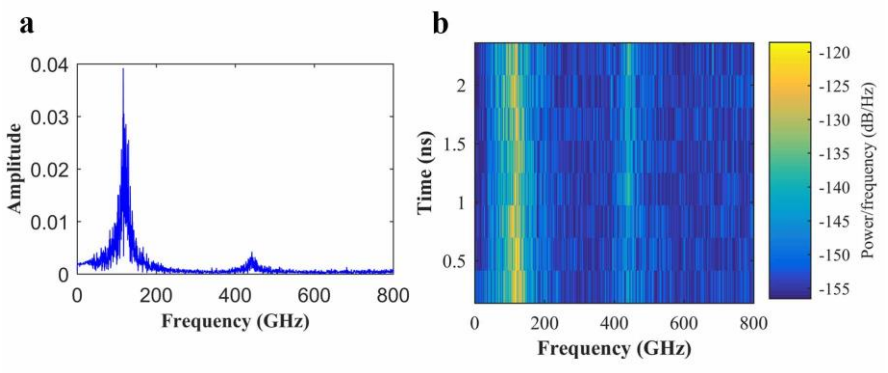


***Figure 4-15*** *Frequency characteristics of CNT with $N_2$ adsorption.* ***(a)*** *The FFT result of the time-displacement curve from CNT vibration in 1 bar $N_2$ at 100K;* ***(b)*** *the STFT result of the same curve.*

### 4.3.2 Influence Factors in Gas Damping Model

Comparing the time-displacement curves in vacuum and $N_2$, the $N_2$ has a significant influence on the vibrational properties of CNT (shown in **Figure 4-10**). The double-clamped CNT shows clear damping during vibration, which is caused by the CNT intrinsic structure and the clamped ends. The damping caused by the gaseous environment is even larger than the sum of intrinsic damping and structural damping. The damping ratio and the frequency are calculated according to the time displacement curve, using the LDM method for different cases.

***Temperature***

The temperature influence on vibration is studied at 1 bar, and compared with the vibration in vacuum, is shown in **Figure 4-16**. Since the system is excited in four different directions, the results for different direction excitations are presented as error bars in **Figure 4-16**, and the markers are the average values for the same case.

When the temperature rises from 100K to 400K, the damping ratio of CNT in the vacuum increases from $1.18 \times 10^{-4}$ to $5.01 \times 10^{-4}$. For the damping in the $N_2$ with full adsorption, the damping ratio generally decreases with the temperature, but the damping ratio increases from 150K to 200K, as shown in **Figure 4-16a**. For the

CNT with only inside-adsorbed molecules, the damping ratio first increases until the temperature reaches 200K, after which the damping ratio decreases with the temperature, as shown in **Figure 4-16b**. For the case with only outside molecules, the damping ratio drops sharply from 100K to 150K, and after that, the damping ratio decreases slowly, as shown in **Figure 4-16c**. No matter what kind of adsorption, the damping ratio approaches the CNT damping in vacuum with the increase of temperature.

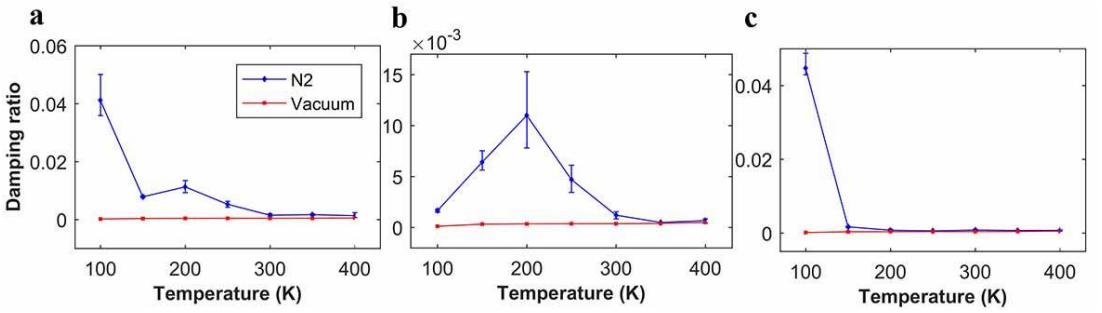


***Figure 4-16*** *The temperature influence on the damping ratio of* ***(a)*** *full adsorption model* ***(b)*** *inside adsorption model* ***(c)*** *outside adsorption model.*

For the CNT vibrating in vacuum, the natural frequency shows minimal changes with temperature, which fluctuates around 141.5 GHz (shown in **Figure 4-17**). For the vibration in $N_2$, the natural frequency shows large changes with temperature. As shown in **Figure 4-17a**, the adsorption lowered the natural frequency, and the frequency gradually approaches the value obtained in vacuum conditions when the temperature increases.

The frequencies of the CNT with only inside or outside adsorption are also examined. As shown in **Figure 4-17b**, the natural frequency for the CNT with only inside adsorption increases significantly in the beginning with the temperature. When the temperature reaches around 300 K, the natural frequency saturates at a value slightly smaller than that under vacuum conditions. Similar results are also found for the CNT with only outside adsorption (**Figure 4-17c**), which shows a much earlier saturation at around 150 K.

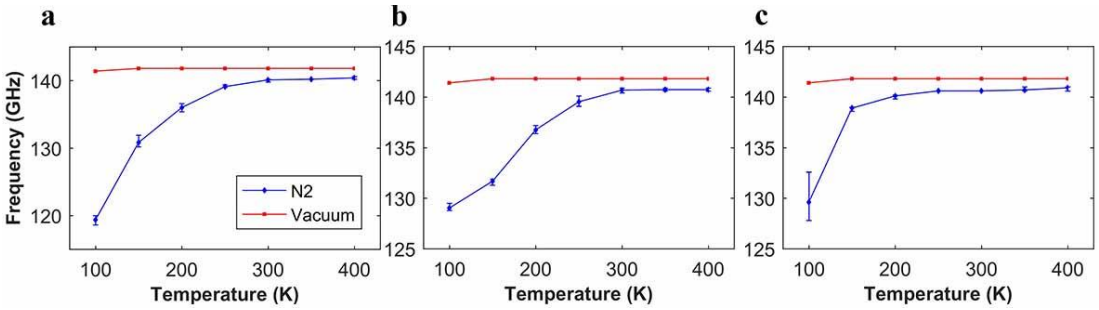


***Figure 4-17*** *Frequency change with temperature from* ***(a)*** *full adsorption model* ***(b)*** *inside adsorption model* ***(c)*** *outside adsorption model.*

The natural frequency of the CNT under the vacuum condition is 141.8GHz from 150K to 400K. Using the equation in Treacy's work, the Young's modulus of CNT is 2.59 TPa, which is in the terapascal range, and consistent with previous experimental work [59]. The damping ratio in vacuum is converted to a quality factor using $Q = \frac{1}{2\zeta}$ and is plotted with $kT^{-0.36}$ curve, as illustrated in **Figure 4-18**. The quality factors are from below 1000 (400K) to more than 4000 (100K), and from 150K to 400K the quality factors fit the $T^{-0.36}$ law well. Generally, lowering the temperature can increase the quality factor for CNT vibration, which is consistent with Lassagne's work [70]. The simulation shows a larger quality factor compared with Lassagne's experimental work; e.g., 50~ 200 at room temperature and 800 ~ 800 at 20K. The agreement between the current simulation with the $T^{-0.36}$ law (between 150 K and 400 K) is also consistent with the silicon wire vibration experiments [66], CNT vibration experiments [71], and also the simulation on CNT vibration [77]. As Young's modulus calculated from the frequency is consistent with the experiment, and the damping ratio trend almost fits the $T^{-0.36}$ law, the vibration simulation and the damping ratio calculation method are reliable in vacuum.

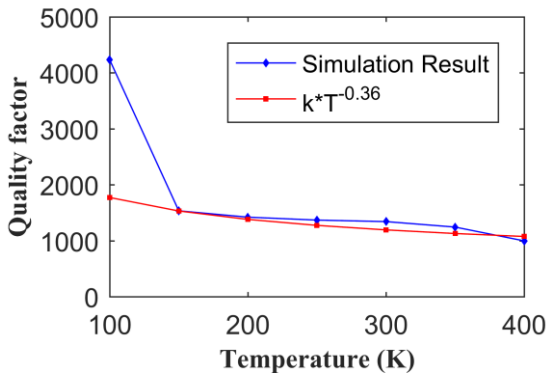

***Figure 4-18*** *Quality factor of pure CNT change with temperature comparing with the* $T^{-0.36}$ *law.*

Comparing the results in gaseous environment with previous CNT vibration tests in atmosphere, which were mostly around 20 [73] or 40 [74], the results for $N_2$ at 300K and 1bar give a quality factor of around 350, which is 10 times higher than for previous experiments. Considering the difference in calculation methods (the current damping ratio calculation method is in the time domain, and the experiment used the frequency domain), the damping ratio is recalculated in the frequency domain from the FFT result and the quality factor is around 140, but it is still higher than the experimental results. Such inconsistency can be caused by the following factors:

1 The excitation in the experiment is usually larger than that in the simulation. In the experiment, a larger displacement is easier to identify and measure, while in the simulation the excitation is smaller, in order to neglect the non-linear factors in vibration. A larger displacement might cause stronger gas damping.

2 The CNT used in experiment is usually multiwall CNT (MWCNT), and the current simulation is for SWCNT. The MWCNT not only has damping from the air, but also has damping between each wall. Also, in the experiment, the MWCNT usually has a lot of defects, which can increase the damping.

Although the damping ratio value in simulation is inconsistent with previous experiments, the changing tendency agrees with experimental measurements. Thus, the discussion and analysis are still valid. One interesting finding is that the sum of the damping ratio for CNTs with only inside and outside adsorption equals to the full adsorption case. As illustrated in **Figure 4-19**, these two values are almost overlapping at all examined temperature values ranging from 100 K to 400 K.

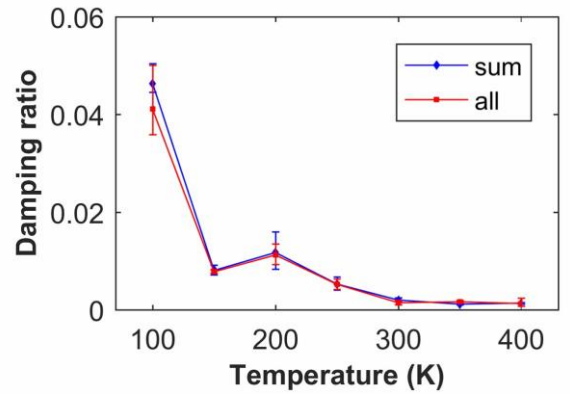


***Figure 4-19*** *Comparison between the damping ratio from the sum of inside and outside and from the overall gaseous environment.*

Recall **Figure 4-16**; the damping ratio for the CNT with only outside adsorption decreases continuously with the temperature. However, the damping ratio for the CNT with only inside adsorption shows an increasing damping ratio from 100K to 200K, which decreases after 200K. Since the damping ratio for the CNT with only outside adsorption is relatively small after 150K, the overall damping ratio is dominated by the inside gas after 150K. Thus, an increasing damping ratio is observed for temperatures ranging from 150 K to 200 K. Generally, temperature can influence the damping in two ways: the number of adsorbed gas molecules in the system, and the thermal motion of the gas molecules.

For the CNT with only outside adsorption, the adsorption amount is decreasing with the temperature and the damping ratio is also decreasing. The enhanced damping effect brought by the thermal motion at higher temperatures is not obvious compared with the damping effect originating from the number of gas adsorbates. According to the kinetic theory of gases, the number of collisions between gas and CNT is proportional to the product of gas molecules' number and average speed of gas molecules. The average speed of gas is proportional to the square root of temperature. Since the increase is only the square root with the temperature but the decrease is in an almost exponential rate, the decrease is the dominant trend. To prove this, the collision parameter with the damping ratio is plotted in **Figure 4-20**. Here, the collision parameter is calculated from $T^{\frac{1}{2}} * N$. As expected, the collision parameter decreases with temperature. For temperatures above 150K, the damping ratio and collision parameter exhibit a nearly linear relation with the temperature. For the case with only outside adsorption, the damping ratio increases with the collision parameter.

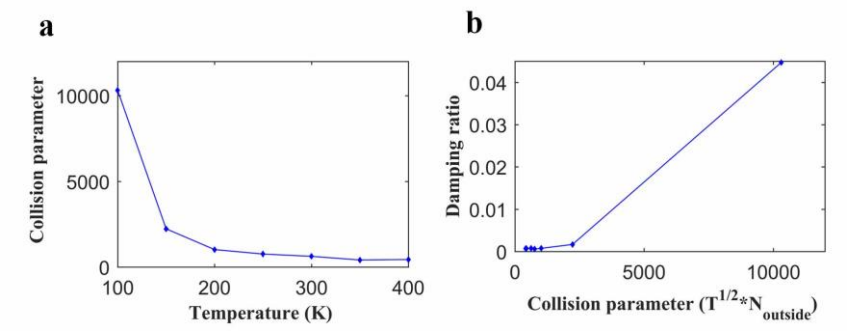


***Figure 4-20 (a)*** *The relation between collision parameter and temperature in outside adsorption model;* ***(b)*** *the relation between damping ratio and collision parameter in outside adsorption model.*

For the CNT with only inside adsorption, the damping mechanism is different. As shown in **Figure 4-21**, the collision parameter decreases continuously with the temperature, which has a non-monotonous relationship with the damping ratio. One obvious conclusion is that after the critical point, higher collision incidents will lower the damping ratio for the CNT with only inside adsorption.

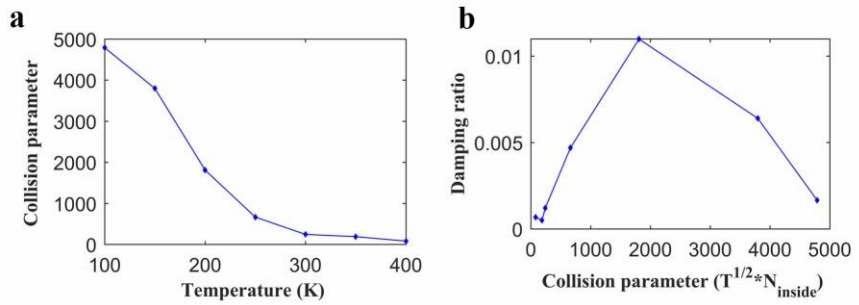


***Figure 4-21 (a)*** *The relation between collision parameter and temperature in inside adsorption model;* ***(b)*** *the relation between damping ratio and collision parameter in inside adsorption model.*

To investigate the configuration of inside adsorption, the normalised radial distribution function (RDF) of $N_2$ is calculated. As shown in **Figure 4-22**, the cut off of the LJ potentials between gas molecules is 10Å, so the distribution farther than 10Å is not calculated. The first peak in the graph is the bond distance for nitrogen. When the temperature is below 200K, the gas molecules are close to each other, and the interaction between gas molecules cannot be ignored. Above 200K, there is no obvious

peak other than the bonding peak, so the collision between gases can be ignored. It is found that 200K is a critical temperature for the inside adsorption configuration, which also corresponds to the peak damping ratio for the CNT with only inside adsorption. It can be concluded that the collisions between the inside gas molecules can lower the damping ratio. If approximating the CNT with inside gas molecules as a composite nanowire in vacuum, different adsorption configurations can be regarded as the existence of inner defects. In this regard, the experimental work of silicon beam vibration in vacuum also discovered a dissipation peak at 160~190K range [64].

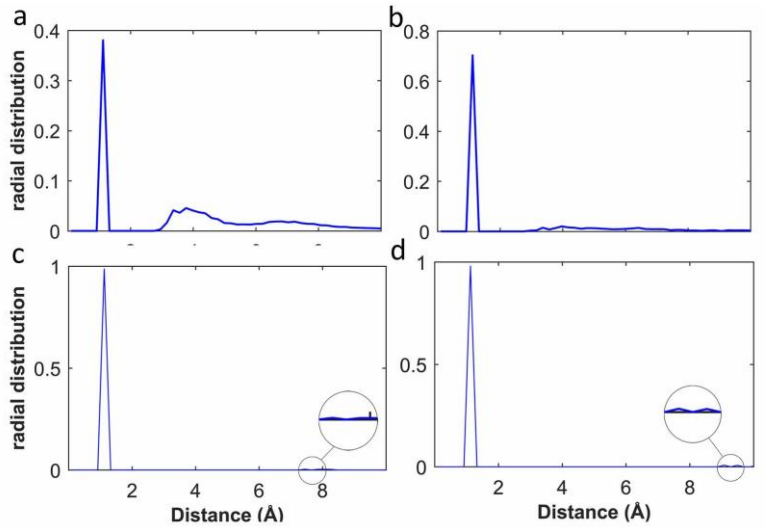


***Figure 4-22*** *RDF of nitrogen inside CNT at the temperature of* ***(a)*** *100K* ***(b)*** *200K* ***(c)*** *300K* ***(d)*** *400K.*

Based on the assumption that collisions between gas molecules and SWCNT have a positive effect on the damping ratio, but the collisions between gas molecules have a negative effect, the simulation result can be fitted using the following model.

$$C = N(T) * \sqrt{T} \tag{4-1}$$

$$\zeta = \frac{aC^2}{C^4 + b} \tag{4-2}$$

where $C$ is the collision parameters which can be used for collisions between the gas molecules and CNT as well as collisions between gas molecules. According to gas kinetic theory, the collision frequency between gas and container is proportional to $C$, and the collision frequency between gas is proportional to $C^2$. The $C^2$ on the numerator presents collisions between the gas molecules and CNT. The $C^4$ on the denominator presents collisions between the gas molecules. Here a quadratic relation

is used between damping and collision frequency, because it fits better than a linear relation. $N(T)$ is the inside adsorbed gas molecule number, $T$ is the temperature, $\zeta$ is the damping ratio, $a$ is the coefficient for each collision effect on the damping ratio, and $b$ is the coefficient related to geometry and structure. As shown in **Figure 4-23**, the simulation results can be fitted by the relationship described by Eq. 4-2.

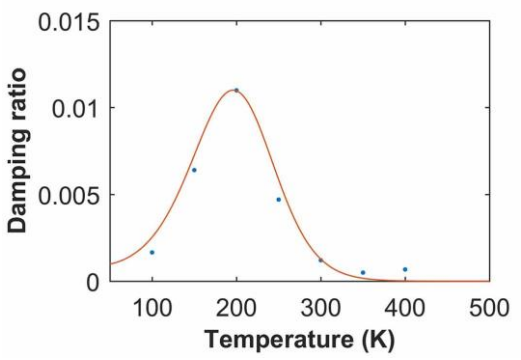


***Figure 4-23*** *Fitting curve from proposed model, compared with the simulation result point.*

Comparing the mathematical model with the expression of dissipation calculation for an anelastic material, which is $Q_T^{-1} = \Delta_M \frac{\omega\tau}{1+(\omega\tau)^2}$ [46], the two expressions are similar in format though they were derived from completely different principles. Thus, another explanation for the damping ratio peak at 200 K is that the inside gas molecules and the CNT behave like an anelastic nanowire in vacuum as a whole, which also agrees with the adsorption model. A further investigation on the anelastic property of the adsorption model and its relation with collision parameters are left for future work.

It is found that the overall damping ratio for the CNT with full adsorption can be obtained by considering the vibration of CNT with only inside and outside adsorption separately. The damping effect is dominated by outside adsorption when the temperature is below 150 K, and the inside adsorption starts to play a dominant role at higher temperatures.

***Pressure***

To study the pressure influence, the system temperature is kept at 100 K, at which temperature the CNT has a significant amount of inside and outside adsorption. As shown in **Figure 4-24a, c**, with the increase of pressure, the vibration frequency decreases for the CNT with full adsorption and only outside adsorption, and the

amount is similar. In comparison, the frequency change is not obvious for the CNT with only inside adsorption, which fluctuates around 129 GHz (shown in **Figure 4-24b)**. The damping ratio for the CNT with full and only outside adsorption increases with the pressure as shown in **Figure 4-24d, f**. On the other hand, the CNT with only inside gas adsorption shows a decreasing damping ratio (shown in **Figure 4-24e)**.

Compared with the damping ratio for the CNT with only outside adsorption, the damping ratio is 10 times smaller for the case with only inside adsorption, indicating the dominant role of outside adsorption. For the CNT with only gas inside the CNT, the damping ratio decreases initially and then saturates at around $1.5 \times 10^{-3}$, which further affirms that when molecules are getting too close together, the damping ratio will decrease. Since the adsorption number shows minor changes for the inside molecules under different pressure values and the molecules are close to each other, the natural frequency for the CNT with only inside adsorption fluctuates at 129 GHz. It is expected that pressure will have different effects on the damping ratio and natural frequency at different temperature values due to the different adsorption configurations. At 100 K the inside adsorption is already significant at 0.2 bar, and the adsorption structure remains unchanged. For other temperatures with a lower adsorption amount, the system is likely to have a critical pressure at which the adsorption structure changes.

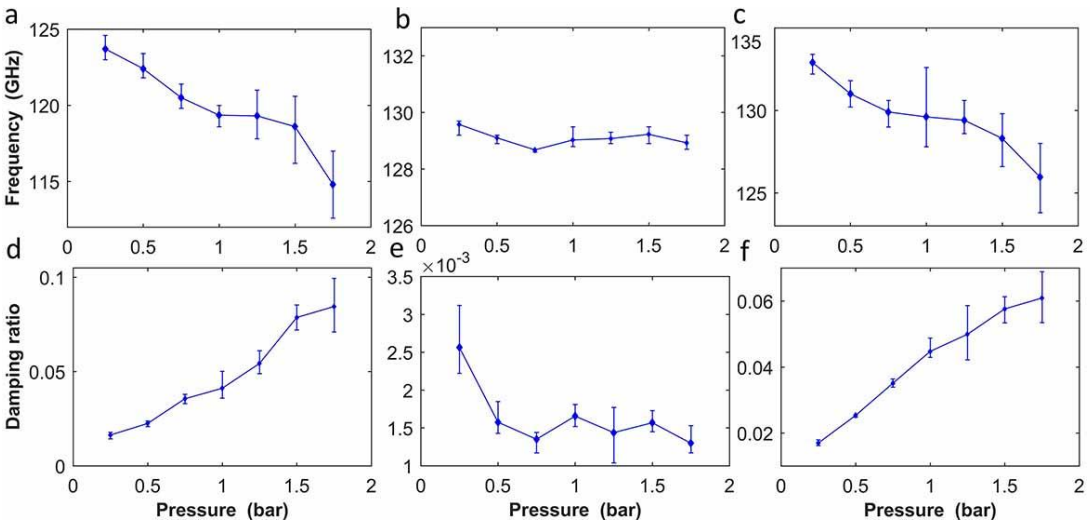


***Figure 4-24*** *The frequency change with the gas pressure for* ***(a)*** *full adsorption model* ***(b)*** *inside adsorption model* ***(c)*** *outside adsorption model; the damping ratio change for* ***(d)*** *full adsorption model* ***(e)*** *inside adsorption model* ***(f)*** *outside adsorption model.*

***Mixture***

The vibration tests for the CNT with the $N_2$-$O_2$ mixture adsorption model are also conducted at the temperature of 100 K and pressure of 1 bar. The natural frequency and the damping ratio show a linear relationship with the percentage of $N_2$ as illustrated in **Figure 4-25**. Similar to the above observation, the CNT with full adsorption shows the same changing tendency in the case with only outside adsorption, and the CNT with only inside adsorption exhibits a different trend. In detail, the frequency decreases when the $N_2$ percentage increases for the CNT with full and outside adsorption (**Figure 4-25a, c)**, and the CNT with only inside adsorption shows an increasing natural frequency. As illustrated in **Figure 4-25d, e, f,** the damping ratio shows an opposite changing tendency. In addition, the outside adsorption is also found to exert a dominant damping effect on the vibrational properties of CNT.

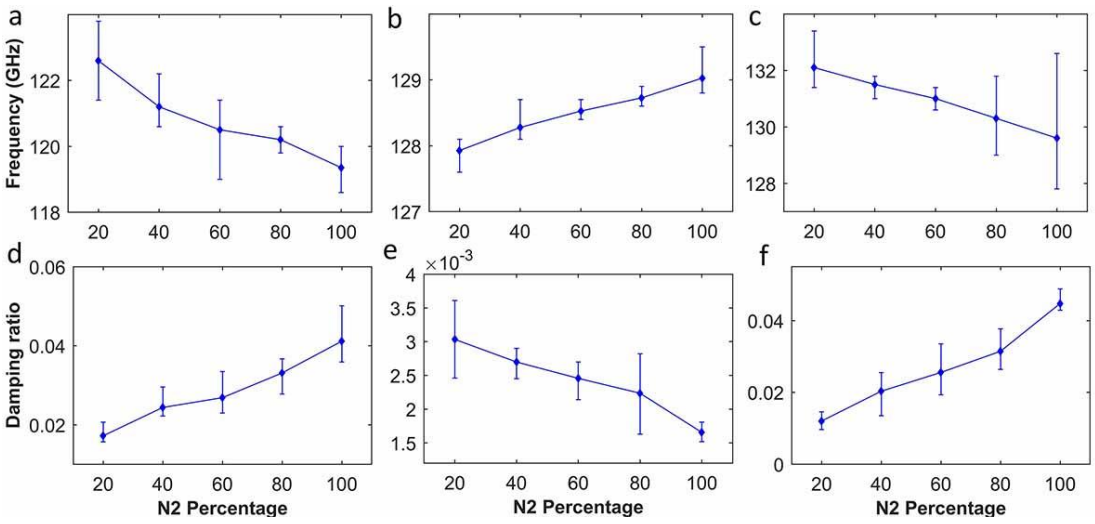


***Figure 4-25*** *The frequency change with the $N_2$ percentage in $N_2$-$O_2$ mixture for* ***(a)*** *full adsorption model* ***(b)*** *inside adsorption model* ***(c)*** *outside adsorption model; the damping ratio change for* ***(d)*** *full adsorption model* ***(e)*** *inside adsorption model* ***(f)*** *outside adsorption model.*

The decreasing natural frequency for the CNT with full adsorption is reasonable due to the fact that a higher amount of adsorption occurs with a higher percentage of $N_2$. However, the frequency increases for the case with only inside adsorption, which still requires further study. Due to the larger amount of gas adsorption at the outside surface of CNT for a higher percentage of $N_2$, the damping ratio increases for the CNT vibration with full adsorption or only outside adsorption. For the case with only inside

adsorption, the damping ratio decreases with the increasing $N_2$ percentage. It is found that the $O_2$ induces a stronger damping effect when molecules are trapped inside the CNT compared with outside adsorption. For outside adsorption, the increase of $O_2$ percentage decreases the adsorbed molecule number and decreases the damping ratio.

### 4.3.3 Conclusion

Overall, the gas adsorption results in the beat phenomenon and a frequency shift to the CNT-based vibration system. Due to the frequency shift, the calculation of the damping ratio is more reliable in the time domain than in the frequency domain. Generally, the adsorption lowers the vibration frequency and increases the damping ratio, and the CNT with full adsorption always has a lower frequency and a higher damping ratio than the scenario with either only inside or outside adsorption. It is found that in some circumstances for the CNT with only inside adsorption, the frequency increases with the adsorption amount. This effect is caused by the adsorption configuration change, and the collision between the inside molecules can lower the damping ratio and improve the frequency and quality factors. Besides the adsorption configuration, the gas type can also influence the vibration properties of the CNT-based resonator.

# Chapter 5: Electric Field Simulation

In this chapter, the results of dynamic electric field simulation (including the charge distribution by AMT and the motion of the CNT by MD simulation) in NEMCS will be presented (Section 5.1). Further discussion and evaluation of the electric field simulation results will be given, and comparisons made with previous works (Section 5.2).

## 5.1 ELECTRIC FIELD SIMULATION

The NEMCS system is built according to the demonstration in Chapter 3. The CNT is fixed at end ***c*** (shown in **Figure 5-1**). To show the improvement of the current simulation method, the graphene electrode is only fixed at two ends ***e, f***. The middle part of the graphene electrode can actually move towards the CNT, driven by electrostatic force, which cannot be presented by the previous model and can lower the pull-in voltage.

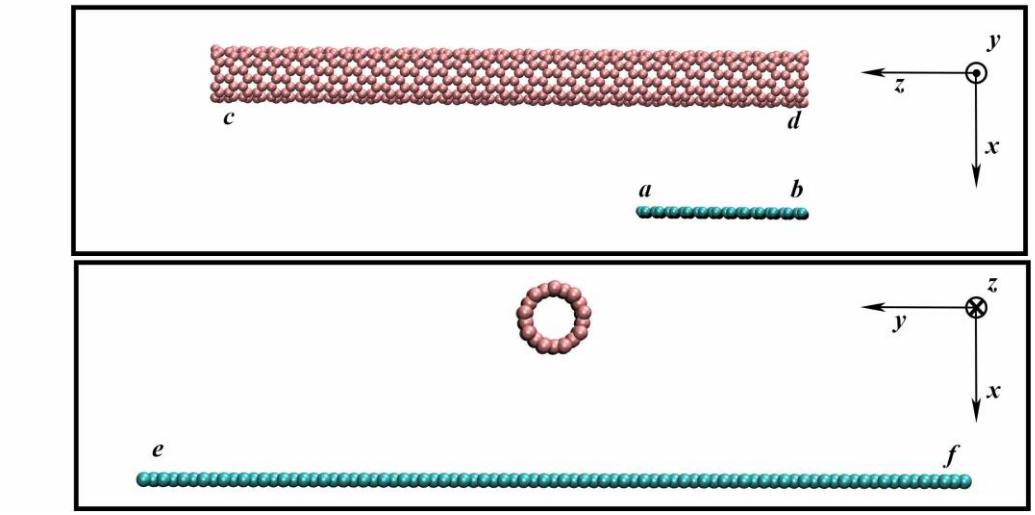


***Figure 5-1*** *The initial MD model for NEMCS. The cyan molecule is the graphene electrode, and the pink molecule is the CNT cantilever.*

### 5.1.1 Charge Distribution Calculation

The AMT method is adopted to calculate the charge distribution on each carbon atom. A 3D image of charge distribution is plotted as shown in **Figure 5-2**, which shows the charge distribution of the (5, 5) CNT at a voltage of 30 V. Here, the initial

distance in the ***X*** direction between the centre of the CNT and graphene is 20 Å. The initial model is obtained after relaxation without charge, in which, the cantilevered CNT is slightly bent and the graphene electrode has some deformation. The blue colour presents the positive charge and the red presents the negative charge. The charge concentration is clearly shown at the tips of CNT and the edge as well as the central portion of the graphene electrode.

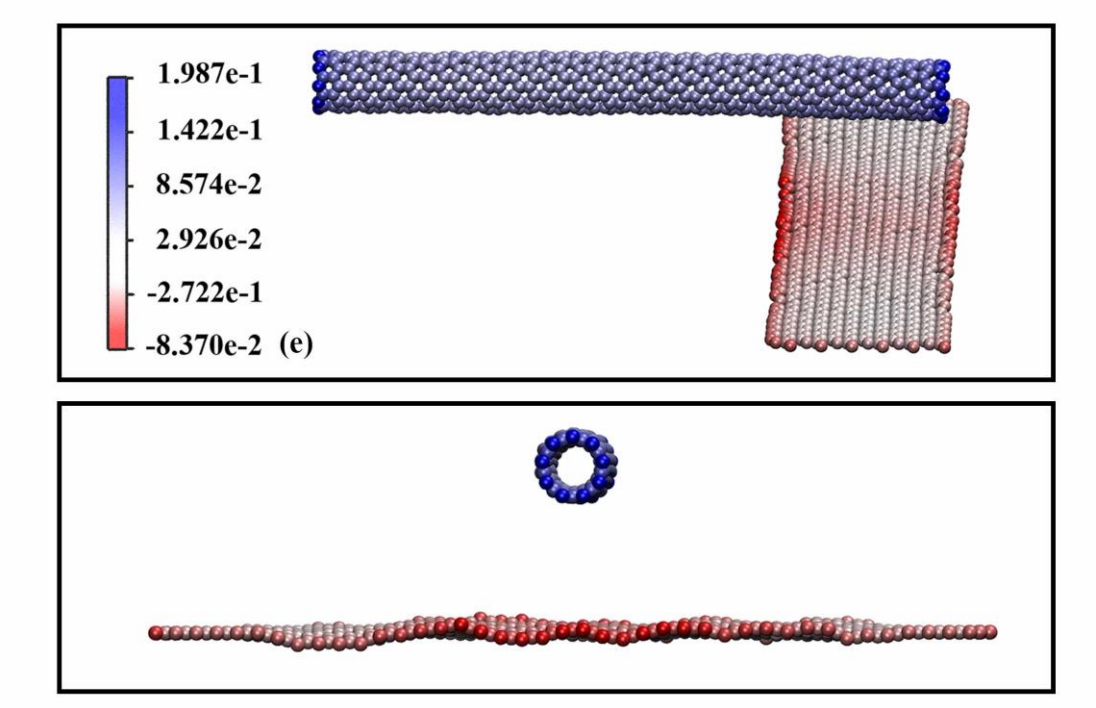


***Figure 5-2*** *The 3D charge distribution on each carbon atom calculated by AMT method. Using BWR colour scale, the blue is positive charge and the red is negative charge.*

To quantify the results in more detail, the charge value is plotted according to the position in the Z direction (shown in **Figure 5-3**). Consistent with the 3D image, there is a charge concentration at the two ends of the CNT, and the atoms at the movable end ***d*** (closer to the graphene electrode, shown in **Figure 5-1**) have a higher charge than the atoms at the fixed end ***c***. Such concentration is significant for atoms whose distance to the tip is within around 5 Å. For the rest of the atoms on the CNT, the maximum atomic charge on each ***Z*** position shows a clear decreasing trend, and this trend differs according to the positions relevant to the graphene electrode. For atoms which have the electrode beneath them and are not influenced by the tip concentration effect (***Z*** position from around 5 to 25), the maximum charge on each ***Z***

position shows a slight decrease, and the maximum charge and the minimum show a large difference. For atoms which don't have an electrode beneath them but are still influenced by the electrode (***Z*** position from around 25 to 50), the difference between the maximum and minimum charge gradually decreases. The maximum charge decreases more rapidly than the minimum and also more rapidly than atoms above the electrode. The minimum charge almost remains the same. For atoms far away from the electrode and not influenced by the tip effect from ***c*** (***Z*** position from around 50 to 80), the maximum charge and minimum don't have much difference, and saturate around 0.05e. These results indicate that atoms at the end closer to the electrode have a higher and wider charge distribution.

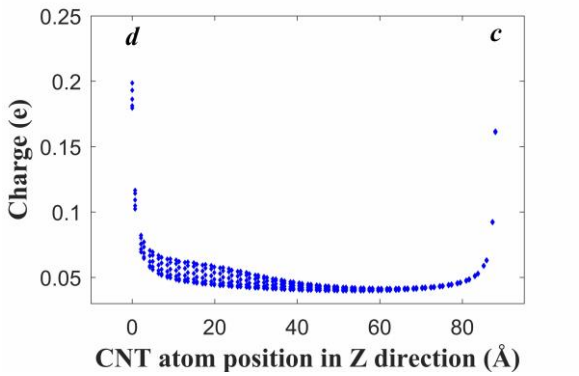


***Figure 5-3*** *CNT charge distribution in Z direction.*

To find out the positions of maximum and minimum charge on each ***Z*** position, the CNT charge distribution is plotted in the other two directions (shown in **Figure 5-4**). In the ***X*** direction, comparing with the ***Z*** distribution in **Figure 5-3**, the tip atom charge values can be identified (shown in **Figure 5-4a**). At moveable tip ***d***, the charge value decreases with the increasing distance to the electrode. For atoms at fixed tip ***c***, the charge remains the same in the ***X*** direction, because the difference in the ***X*** direction is relatively small compared with the distance to the electrode. In the ***Y*** direction, the charge shows a symmetrical distribution (shown in **Figure 5-4b**) consistent with the system set up. All the observable characteristics of the result are consistent with the preconceptions for charge distribution.

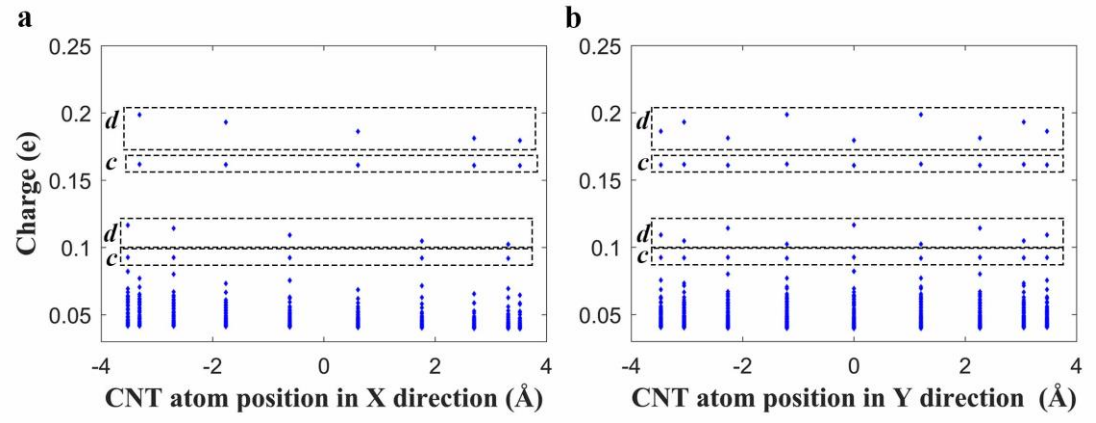


***Figure 5-4*** *The CNT charge distribution in X (**a**) and Y (**b**) directions. The dotted boxes show the atom positions at tip **c** or tip **d**.*

The charge distribution on the graphene electrode is also calculated and plotted with the same method. The charge on the electrode has a negative value, which is opposite to the CNT (shown in **Figure 5-5**). The charge distribution in the ***Y*** direction shows a concentration in the middle part of the graphene sheet where the CNT locates. The two edges of the electrode also show a charge concentration phenomenon, which is less significant than the middle part. Overall the distribution in the ***Y*** direction is symmetrical, and is consistent with the model.

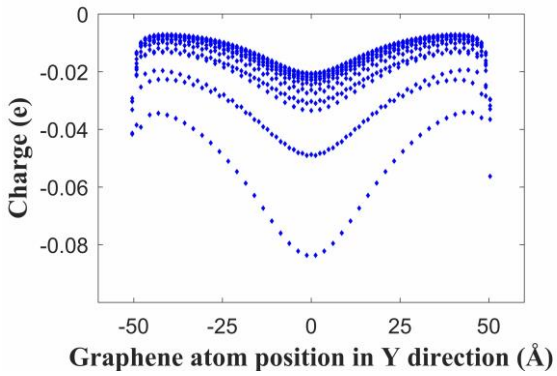


***Figure 5-5*** *The charge distribution on graphene electrode in Y direction.*

Similar to the charge distribution in the ***Y*** direction, the charge distribution on the electrode in the ***Z*** direction also shows a concentration effect at the two edges. However the distribution is asymmetrical (shown in **Figure 5-6**). Since the CNT is longer than the electrode, and the edge ***a*** (actual position shown in **Figure 5-1**) has a larger concentration than the edge ***b***, because for atoms at edge ***a***, they have more positively charged CNT atoms near them.

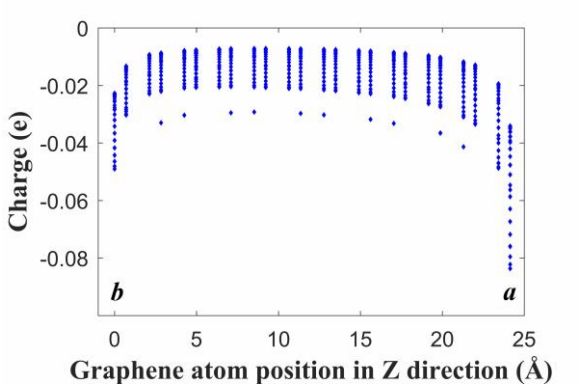


***Figure 5-6*** *Charge distribution on electrode in* ***Z*** *direction.*

### 5.1.2 Pull-in Simulation

With the above initial charge distribution calculation, the whole system will undergo pull-in simulation. Due to the Coulombic force or electrostatic interaction, the CNT and the graphene will move towards each other. During such a process, the charge distribution must be updated.

To eliminate the influence of thermal fluctuation and local deformation, a group of atoms at the tip ***d*** (72 atoms, the minimum structure period in CNT axial direction) are defined as tip atoms, and used to study the dynamic properties of a NEMCS system. The trajectory of the mass centre of the tip atoms is tracked to inspect the displacement of the CNT tip. As compared in **Figure 5-7**, the CNT will exhibit different movement trajectories when the charge update frequency changes. The results show a converging tendency when the update frequency is below 0.1 ps. Specifically, the displacement of the CNT with a higher update frequency usually is larger than the case with a lower update frequency. In addition, without charge update, there is a platform stage of displacement at around 2 ps during the pull-in process. However, such a platform is eliminated by a charge update in other curves. Since the gap between the CNT mass centre and graphene electrode is 20 Å, the pull-in time should be when the displacement of the tip mass centre reaches 20 Å minus the radius 3.5 Å, which is when the bottom atoms touch the graphene electrode. Since the graphene sheet is clamped at both ends, not the whole sheet, the middle part of the graphene will come to the CNT slightly during the pull-in process. Without charge update, the result for pull-in time is around 3 ps, and with charge update, the pull-in time is around 2 ps. Estimation of the pull-in time without the update of charge can generate a 50% error, which can result in error for prediction of other dynamic properties for NEMCS.

The simulation box is 40 Å larger than the NEMCS system in each dimension (shown in Section 3.4), and the graphene is only fixed at the two edges, which allows for motion exceeding 20 Å after the pull-in process. In NEMCS, after the CNT and graphene contact with each other, the potential difference does not exist instantly, which is used to calculate the charge distribution in AMT method. This means that the AMT method does not have the ability to calculate the electric field after pull-in. Although the AMT results after pull-in are not the actual motion, this is not what the model is built for, and the results are just kept for comparison and convergence study.

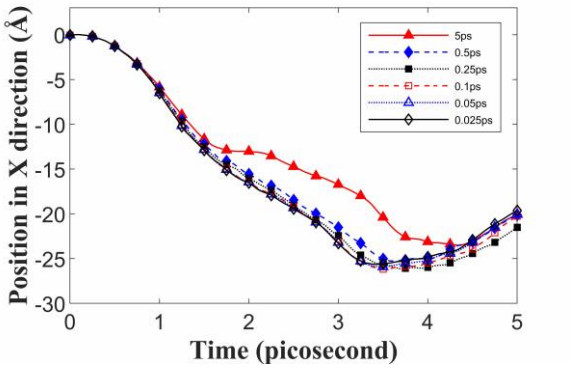


***Figure 5-7*** *The motion of the mass centre of the tip atoms by different charge update frequencies*

The displacement of the CNT tip decreases after the pull-in because the final configuration of the system is the CNT and the graphene sheet vibrating together. To highlight the limitation of AMT method, the configuration of CNT-graphene have been analysed. When the charge is not updated by AMT, the final configuration is the CNT attached to the graphene electrode, and they are vibrating together (**Figure 5-8a**). If the charge is updated by AMT, the CNT will grasp the graphene sheet and vibrate together (**Figure 5-8b**). As previously mentioned, the potential difference vanishes when the CNT adheres to the graphene sheet, and the charge calculation on the atom by AMT is no longer valid, thus both configurations are not physically valid.

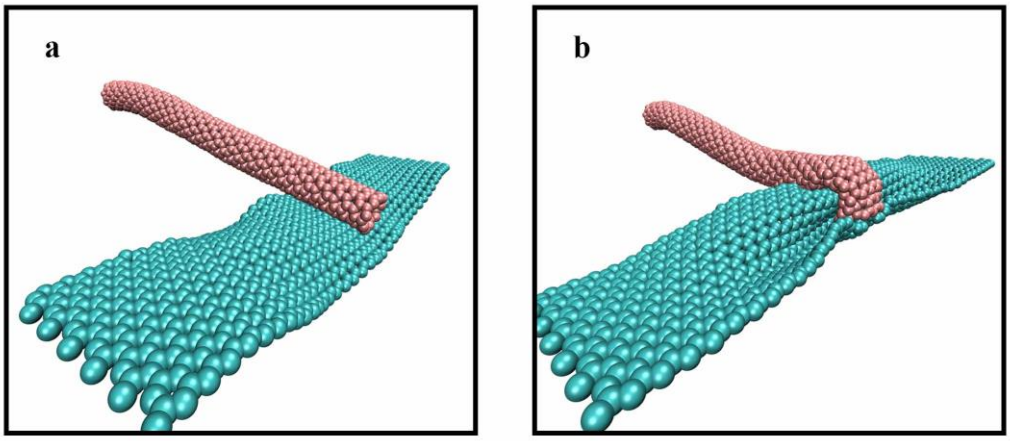


***Figure 5-8*** *The configuration at 5ps* ***(b)*** *with and* ***(a)*** *without charge update.*

The sum of charge of the tip atoms is tracked in following **Figure 5-9**. Without any update, the sum of charge is around 4 e, which will remain unchanged. The sum of charge increases significantly when updated. Simulation shows that the CNT will be completely pulled in at around 2 ps. When the charge is updated, the final charge in the pull-in process is more than 2 times the initial settings. The increase of charge sum can increase the electrostatic force, which eliminates the platform stage in the displacement curve, and results in a shorter pull-in time. The tracked group of atoms exhibits a different charge variation profile when the charge update frequency changes. Such results indicate the importance of charge update during the simulation of resonators in a charged environment. Similar to the displacement curve, the charge results also show a convergent tendency when the update frequency is below 0.1 ps.

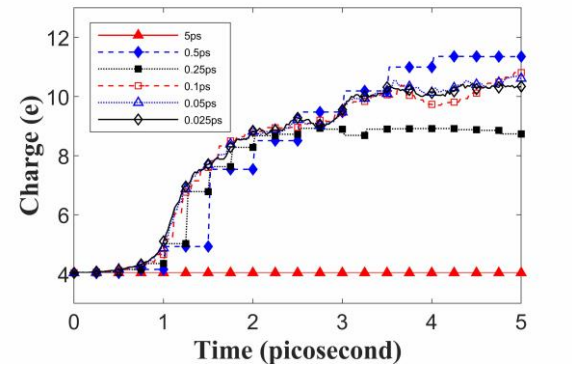


***Figure 5-9*** *The sum of charge values of tip atoms by different charge update frequency*

To test the convergent properties of the current simulation, the motion and charge of one single atom at the tip are tracked, and are more strict than for the sum of

a group of atoms. They all show a convergent trend when the update frequency is below 0.1 ps (shown in **Figure 5-10**).

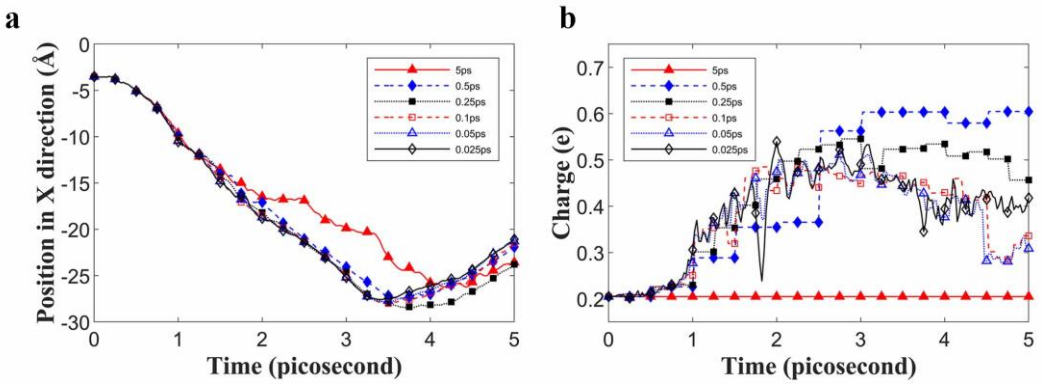


***Figure 5-10*** *The motion* ***(a)*** *and charge information* ***(b)*** *of a single atom at tip.*

## 5.2 DISCUSSION

The above results show that the pull-in behaviour of the CNT-based NEMCS differs significantly when the charge distribution update is considered. However, it is noticed that most previous studies used a guessed and fixed charge distribution without considering the pull-in voltage [5], [10], [22]. Since MD can provide detailed structure information at the atomistic level, several MD works discuss the defect influence on the pull-in charge. Without charge update, Fakhrabadi [5] found that there are three pull-in stages in the CNT-based NEMCS system, as shown in **Figure 5-11**. It is expected that without charge update, the electrostatic force increment is smaller compared with the elastic restoring force increment, and thus results in the three-stage pull-in process. With the updated charge distribution, the atom charge at the tip region increased during the pull-in process, which will thus create a stronger electrostatic force. In this case, the second stage will disappear.

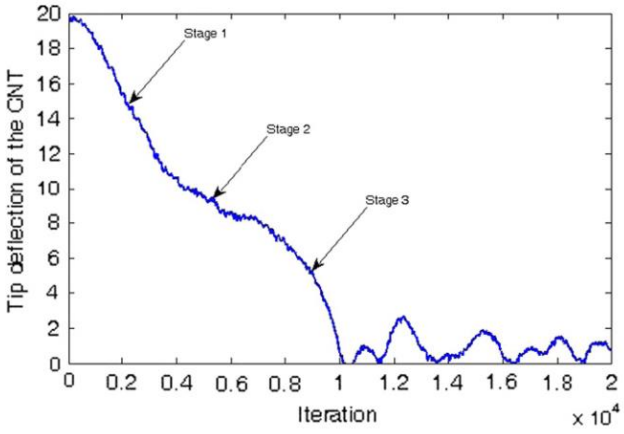


***Figure 5-11*** *The three stage tip deflection* [5]

Overall, the charge distribution plays an important role in describing the dynamic properties of NEMCS during the pull-in process. The update frequency of 0.1ps can give a satisfying prediction of the motion of the CNT tip (free end).

# Chapter 6: Conclusions and Limitations

## 6.1 CONCLUSIONS

In this work, multiple theories are adopted to develop a multiphysics model for a CNT based NEMCS system working in a gaseous environment. Based on the MD method, the AMT approach is used to simulate the electric field, and the GCMC method is used to simulate adsorption in gaseous environments. From the studies in this project, the following conclusions have been drawn:

- The gas adsorption happens on both inner and outer surfaces of the open-end CNT (with a relatively large diameter) and shows different adsorption models. The outside gas adsorption is similar to the type I adsorption model, while the inside is similar to the type V, which has a second adsorption layer.
- Due to the different adsorption configurations, the inside adsorption amount can be larger than the outside case at certain temperatures (though the area is smaller for inside adsorption).
- Adsorption changes the CNT into an asymmetric structure, and causes a beat phenomenon and frequency shift; it is more appropriate to calculate the damping in the time domain than in the frequency domain.
- Inside and outside gas adsorption will result in different influences on the damping ratio and natural frequency of the vibration system. Outside adsorption dominates the damping effect at around 150K, while inside adsorption dominates when the temperature is higher. The damping and frequency is not purely determined by the adsorption amount, but also influenced by the adsorption configuration.
- The damping caused by inside gas adsorption shows a maximum value at 200K, which is also the critical point for the change of adsorption configuration.
- The dynamic electric field calculation can give a convergent result, which is better than the results from previous work using a static electric

field. The tip charge concentration increases with the bending process of the CNT, and the dynamic electric field provides a shorter pull-in time than the static one.

- For the MD simulation of NEMCS, it is better to simulate the pull-in process with a charge distribution update.

## 6.2 LIMITATIONS AND FUTURE WORK

The current simulation establishes an enhanced simulation model for a CNT based NEMCS system, considering charge distribution and its variation as well as the gaseous environment. There are several limitations which require further research:

- In the adsorption simulation, the GCMC method will produce a model with a transient adsorption amount that changes due to thermal fluctuations. Thus, for a valid investigation, it is necessary to carry out a series of simulations on several selected adsorption models.
- Current work studied the open-end CNT; it would be very interesting to probe how the closed-end CNT will perform under a gaseous environment or with an updated charge distribution.
- In the GCMC simulation, many assumptions are adopted: the chemical potential of adsorbate is calculated as an ideal gas; the gas molecules are fixed as rigid; the potential between gas and the inside and outside CNT surface is equal, and no curvature influence is considered on the potential field. How these assumptions influence the results is open for further discussion.
- The mixture adsorption simulation method needs to be improved, in order to realise an accurate interpretation of the percentages of different components.
- In the adsorption vibration model, the method used for damping ratio calculation is LDM in the time domain, which is usually for a linear damping system. To limit the non-linear terms in the damping, a small excitation is used for vibration. Whether the damping effect will be different for a larger excitation and how the vibration amplitude influences the adsorption amount remain questions for future research.

- The combination of adsorption and vibration is achieved, but the combination of electric field and fluid field is still challenging. Although the two scripts can work together, how the electric field will affect the adsorption is not discussed in the current work.
- The charge distribution calculation is based on the assumption that the CNT and graphene are isopotential bodies. Although the (5,5) CNT and graphene have good electric conductivity, while considering the speed of electrons, whether the charge distribution status can change to the next status predicted within the update time needs further evidence from DFT calculations.

# Bibliography


[1] V. De and S. Borkar, "Technology and design challenges for low power and high performance," *Proc. 1999 Int. Symp. Low power Electron. Des. - ISLPED '99*, pp. 163–168, 1999.

[2] O. Loh, X. Wei, C. Ke, J. Sullivan, and H. D. Espinosa, "Robust carbon-nanotube-based nano-electromechanical devices: Understanding and eliminating prevalent failure modes using alternative electrode materials," *Small*, vol. 7, no. 1, pp. 79–86, 2011.

[3] H. J. Hwang and J. W. Kang, "Carbon-nanotube-based nanoelectromechanical switch," *Phys. E Low-Dimensional Syst. Nanostructures*, vol. 27, no. 1–2, pp. 163–175, 2005.

[4] J. W. Kang, J. H. Lee, H. J. Lee, and H. J. Hwang, "A study on carbon nanotube bridge as a electromechanical memory device," *Phys. E Low-Dimensional Syst. Nanostructures*, vol. 27, no. 3, pp. 332–340, 2005.

[5] M. M. S. Fakhrabadi, P. K. Khorasani, A. Rastgoo, and M. T. Ahmadian, "Molecular dynamics simulation of pull-in phenomena in carbon nanotubes with Stone-Wales defects," *Solid State Commun.*, vol. 157, pp. 38–44, 2013.

[6] S. Bornassi and H. Haddadpour, "Nonlocal vibration and pull-in instability analysis of electrostatic carbon-nanotube based NEMS devices," *Sensors Actuators A Phys.*, 2017.

[7] C. Chen, M. Ma, J. Zhe Liu, Q. Zheng, and Z. Xu, "Viscous damping of nanobeam resonators: Humidity, thermal noise, and a paddling effect," *J. Appl. Phys.*, vol. 110, no. 3, 2011.

[8] W. Zhang and K. Turner, "Frequency dependent fluid damping of micro/nano flexural resonators: Experiment, model and analysis," *Sensors Actuators, A Phys.*, vol. 134, no. 2, pp. 594–599, 2007.

[9] C. Ke, H. D. Espinosa, and N. Pugno, "Numerical Analysis of Nanotube Based NEMS Devices — Part II: Role of Finite Kinematics, Stretching and Charge Concentrations," *J. Appl. Mech.*, vol. 72, no. 5, p. 726, 2005.

[10] M. M. Seyyed Fakhrabadi, A. Rastgoo, and M. T. Ahmadian, "On the Pull-in Instability of Double-Walled Carbon Nanotube-Based Nano Electromechanical Systems with Cross-Linked Walls," *Fullerenes, Nanotub. Carbon Nanostructures*, vol. 23, no. 4, pp. 300–314, 2015.

[11] G. Moore, "Progress In Digital Integrated Electronics [Technical literaiture, Copyright 1975 IEEE. Reprinted, with permission. Technical Digest. International Electron Devices Meeting, IEEE, 1975, pp. 11-13.]," *IEEE Solid-State Circuits Newsl.*, vol. 20, no. 3, pp. 36–37, 2006.

[12] International Technology Roadmap for Semiconductors, "Executive summary: Grand challenges," *Itrs*, p. [online] Available: http://www.itrs.net, 2009.

[13] H. F. Dadgour, M. M. Hussain, and K. Banerjee, “A New Paradigm in the Design of Energy-Efficient Digital Circuits using Laterally-Actuated Double-Gate NEMS,” *Low-Power Electron. Des. (ISLPED), 2010 ACM/IEEE Int. Symp.*, pp. 7–12, 2010.

[14] O. Y. Loh and H. D. Espinosa, “Nanoelectromechanical contact switches,” *Nat. Nanotechnol.*, vol. 7, no. 5, pp. 283–295, 2012.

[15] O. Loh, X. Wei, J. Sullivan, L. E. Ocola, R. Divan, and H. D. Espinosa, “Carbon-carbon contacts for robust nanoelectromechanical switches,” *Adv. Mater.*, vol. 24, no. 18, pp. 2463–2468, 2012.

[16] R. F. Smith, T. Rueckes, S. Konsek, J. W. Ward, D. K. Brock, and B. M. Segal, “Carbon Nanotube Based Memory Development and Testing,” *2007 IEEE Aerosp. Conf.*, pp. 1–5, 2007.

[17] S. K. Roy, V. T. K. Sauer, J. N. Westwood-Bachman, A. Venkatasubramanian, and W. K. Hiebert, “Improving mechanical sensor performance through larger damping,” vol. 5220, 2017.

[18] M. Dequesnes, Z. Tang, and N. R. Aluru, “Static and Dynamic Analysis of Carbon Nanotube-Based Switches,” *J. Eng. Mater. Technol.*, vol. 126, no. 3, p. 230, 2004.

[19] M. Dequesnes, S. V Rotkin, and N. R. Aluru, “Calculation of pull-in voltages for carbon-nanotube-based nanoelectromechanical switches,” *Nanotechnology*, vol. 13, no. 1, pp. 120–131, 2002.

[20] J. Yang, X. L. Jia, and S. Kitipornchai, “Pull-in instability of nano-switches using nonlocal elasticity theory,” *J. Phys. D. Appl. Phys.*, vol. 41, no. 3, p. 035103, 2008.

[21] B. J. Alder and T. E. Wainwright, “Studies in molecular dynamics. I. General method,” *J. Chem. Phys.*, vol. 31, no. 2, pp. 459–466, 1959.

[22] S. Hoshyarmanesh and M. Bahrami, “Molecular Dynamic Study of Pull-In Instability of Nano-Switches,” no. August, pp. 122–132, 2014.

[23] Rapaport, D.C., and D. Rapaport, *The Art of Molecular Dynamics Simulation*. Cambridge University Press, 2004.

[24] M. Rasekh, S. E. Khadem, and M. Tatari, “Noise immunity of carbon nanotube based switches,” *ASME 2010 10th Bienn. Conf. Eng. Syst. Des. Anal. ESDA2010*, vol. 5, pp. 1–9, 2010.

[25] S. E. Khadem, M. Rasekh, and A. Toghraee, “Design and simulation of a carbon nanotube-based adjustable nano-electromechanical shock switch,” *Appl. Math. Model.*, vol. 36, no. 6, pp. 2329–2339, 2012.

[26] C. Ke and H. D. Espinosa, “Numerical Analysis of Nanotube-Based NEMS Devices—Part I: Electrostatic Charge Distribution on Multiwalled Nanotubes,” *J. Appl. Mech.*, vol. 72, no. 5, p. 721, 2005.

[27] L. Lou, P. Nordlander, and R. E. Smalley, “Fullerene nanetubes in electric fields,” *Phys. Rev. B*, vol. 52, no. 3, pp. 15–1995, 1995.

[28] P. Keblinski, S. K. Nayak, P. Zapol, and P. M. Ajayan, “Charge distribution and stability of charged carbon nanotubes.,” *Phys. Rev. Lett.*, vol. 89, no. 25, p. 255503, 2002.

[29] C. Li and T.-W. Chou, “Electrostatic charge distribution on single-walled carbon nanotubes,” *Appl. Phys. Lett.*, vol. 89, no. 6, p. 063103, 2006.

[30] M. Jaroniec, X. C. Lu, and R. Madey, “Physical Adsorption of Gases and Vapors On Structurally Heterogeneous Microporous Solids,” *Chem. Scr.*, vol. 28, no. 4, pp. 369–374, 1988.

[31] S. Brunauer, P. H. Emmett, and E. Teller, “Adsorption of Gases in Multimolecular Layers,” *J. Am. Chem. Soc.*, vol. 60, no. 2, pp. 309–319, 1938.

[32] K. S. W. Sing *et al.*, “International Union of Pure Commission on Colloid and Surface Chemistry Including Catalysis-Reporting physisorption data for gas/solid systems with special reference to the determination of surface area and porosity,” in *Pure & Appl. Chem.*, 1985, vol. 57, no. 4, pp. 603–619.

[33] K. Y. Foo and B. H. Hameed, “Insights into the modeling of adsorption isotherm systems,” *Pet. Coal*, vol. 56, no. 5, pp. 552–561, 2014.

[34] J. R. Arnold, “Adsorption of Gas Mixtures. Nitrogen-Oxygen on Anatase,” *J. Am. Chem. Soc.*, vol. 71, no. 1, pp. 104–110, 1949.

[35] T. L. Hill, “Theory of multimolecular adsorption from a mixture of gases,” *J. Chem. Phys.*, vol. 14, no. 4, pp. 268–275, 1946.

[36] A. L. Myers and J. M. Prausnltz, “Thermodynamics of mixed-gas adsorption,” *AIChE J.*, vol. 11, no. 1, pp. 121–127, 1965.

[37] A. Kundu, K. Sillar, and J. Sauer, “Ab Initio Prediction of Adsorption Isotherms for Gas Mixtures by Grand Canonical Monte Carlo Simulations on a Lattice of Sites,” *J. Phys. Chem. Lett.*, vol. 8, no. 12, pp. 2713–2718, 2017.

[38] G. Arora, N. J. Wagner, and S. I. Sandler, “Adsorption and diffusion of molecular nitrogen in single wall carbon nanotubes.,” *Langmuir*, vol. 20, no. 15, pp. 6268–6277, 2004.

[39] J. K. Wang, Qinju; Johnson, “Molecular simulation of hydrogen adsorption in charged single-walled carbon nanotubes and idealized carbon slit pores,” *J. Chem. Phys.*, vol. 111, no. 21, p. 9778, 1999.

[40] Q. Wang and J. K. Johnson, “Hydrogen adsorption on graphite and in carbon slit pores from path integral simulations,” *Mol. Phys.*, vol. 95, no. 2, pp. 299–309, 1998.

[41] A. Amir Abbas, S. Majid Hashemianzadeh, Z. Bolboli Nojini, and N. Naghshineh, “Canonical Monte Carlo Simulation of Adsorption of O2 and N2 Mixture on Single Walled Carbon Nanotube at Different Temperatures and Pressures,” *J. Comput. Chem.*, vol. 28, no. 1, pp. 73–86, 2009.

[42] H. Cheng, A. C. Cooper, G. P. Pez, M. K. Kostov, P. Piotrowski, and S. J. Stuart, “Molecular Dynamics Simulations on the Effects of Diameter and Chirality on Hydrogen Adsorption in Single Walled Carbon Nanotubes,” *J.*

*Phys. Chem. B*, vol. 109, no. 9, pp. 3780–3786, 2005.

[43] R. F. Cracknell, K. E. Gubbins, D. Nicholson, K. E. Gubbins, M. Maddox, and K. E. Gubbins, "Modeling Fluid Behavior in Well-Characterized Porous Materials," *Acc. Chem. Res.*, vol. 28, no. 7, pp. 281–288, 1995.

[44] S. S. Han and H. M. Lee, "Adsorption properties of hydrogen on (10,0) single-walled carbon nanotube through density functional theory," *Carbon N. Y.*, vol. 42, no. 11, pp. 2169–2177, 2004.

[45] C. Zener, "Internal friction in solids II. General theory of thermoelastic internal friction," *Phys. Rev.*, vol. 53, no. 1, pp. 90–99, 1938.

[46] R. Lifshitz and M. Roukes, "Thermoelastic damping in micro- and nanomechanical systems," *Phys. Rev. B - Condens. Matter Mater. Phys.*, vol. 61, no. 8, pp. 5600–5609, 2000.

[47] K. Y. Yasumura *et al.*, "Quality factors in micron- and submicron-thick cantilevers," *J. Microelectromechanical Syst.*, vol. 9, no. 1, pp. 117–125, 2000.

[48] D. A. Czaplewski, J. P. Sullivan, T. A. Friedmann, D. W. Carr, B. E. N. Keeler, and J. R. Wendt, "Mechanical dissipation in tetrahedral amorphous carbon," *J. Appl. Phys.*, vol. 97, no. 2, 2005.

[49] P. w. Anderson, B. I. Halperin, and c. M. Varma, "Anomalous low-temperature thermal properties of glasses and spin glasses," *Philos. Mag. A J. Theor. Exp. Appl. Phys.*, vol. 25, no. 1, pp. 1–9, Jan. 1972.

[50] K. A. Topp and D. G. Cahill, "Elastic properties of several amorphous solids and disordered crystals below 100 K," *Zeitschrift für Phys. B Condens. Matter*, vol. 101, no. 2, pp. 235–245, 1996.

[51] K. H. Ahn and P. Mohanty, "Quantum Friction of Micromechanical Resonators at Low Temperatures," *Phys. Rev. Lett.*, vol. 90, no. 8, p. 4, 2003.

[52] M. C. Cross and R. Lifshitz, "Elastic wave transmission at an abrupt junction in a thin plate with application to heat transport and vibrations in mesoscopic systems," *Phys. Rev. B - Condens. Matter Mater. Phys.*, vol. 64, no. 8, pp. 1–22, 2001.

[53] Z. Hao, A. Erbil, and F. Ayazi, "An analytical model for support loss in micromachined beam resonators with in-plane flexural vibrations," *Sensors Actuators, A Phys.*, vol. 109, no. 1–2, pp. 156–164, 2003.

[54] W. E. Newell, "Miniaturization of tuning forks.," *Science*, vol. 161, no. 3848, pp. 1320–1326, 1968.

[55] G. M. REBEIZ, *RF MEMS-Theory, Design, and Technology*. A JOHN WILEY & SONS PUBLICATION, 2003.

[56] J. Cattarius and D. J. Inman, "Time domain analysis for damage detection in smart structrues," *Mech. Syst. Signal Process.*, vol. 11, no. 3, pp. 409–423, 1997.

[57] S. K. Yalla and A. Kareem, “Beat phenomenon in combined structure-liquid damper systems,” *Eng. Struct.*, vol. 23, no. 6, pp. 622–630, 2001.

[58] J. Weavbr, P. Technology, P. O. Box, and D. Mar, “Nonlinear Vibrations i f a learn With Pinned Ends,” vol. 4, no. May, 1976.

[59] M. M. J. Treacy, T. W. Ebbesen, and J. M. Gibson, “Exceptionally high Young’s modulus observed for individual carbon nanotubes,” *Nature*, vol. 381, no. 6584, pp. 678–680, 1996.

[60] P. Poncharal, Z. L. Wang, D. Ugarte, and W. A. de Heer, “Electrostatic Deflections and Electromechanical Resonanses of Carbon Nanotubes,” *Science (80-. ).*, vol. 283, no. 5407, p. 1513, 1999.

[61] S. Cuenot, C. Frétigny, S. Demoustier-Champagne, and B. Nysten, “Measurement of elastic modulus of nanotubes by resonant contact atomic force microscopy,” *J. Appl. Phys.*, vol. 93, no. 9, pp. 5650–5655, 2003.

[62] A. Eichler, J. Moser, J. Chaste, M. Zdrojek, I. Wilson-Rae, and A. Bachtold, “Nonlinear damping in mechanical resonators made from carbon nanotubes and graphene,” *Nat. Nanotechnol.*, vol. 6, no. 6, pp. 339–342, 2011.

[63] D. W. Carr, S. Evoy, L. Sekaric, H. G. Craighead, and J. M. Parpia, “Measurement of mechanical resonance and losses in nanometer scale silicon wires,” *Appl. Phys. Lett.*, vol. 75, no. 7, pp. 920–922, 1999.

[64] A. Olkhovets, S. Evoy, D. W. Carr, J. M. Parpia, and H. G. Craighead, “Actuation and internal friction of torsional nanomechanical silicon resonators,” *J. Vac. Sci. Technol. B*, vol. 18, no. 6, pp. 3549–3551, 2000.

[65] S. Evoy, A. Olkhovets, L. Sekaric, J. M. Parpia, H. G. Craighead, and D. W. Carr, “Temperature-dependent internal friction in silicon nanoelectromechanical systems,” *Appl. Phys. Lett.*, vol. 77, no. 15, pp. 2397–2399, 2000.

[66] G. Zolfagharkhani, A. Gaidarzhy, S. B. Shim, R. L. Badzey, and P. Mohanty, “Quantum friction in nanomechanical oscillators at millikelvin temperatures,” *Phys. Rev. B - Condens. Matter Mater. Phys.*, vol. 72, no. 22, pp. 1–5, 2005.

[67] J. Yang, T. Ono, and M. Esashi, “Surface effects and high quality factors in ultrathin single-crystal silicon cantilevers,” *Appl. Phys. Lett.*, vol. 77, no. 23, pp. 3860–3862, 2000.

[68] J. Yang, T. Ono, and M. Esashi, “Investigating surface stress: Surface loss in ultrathin single-crystal silicon cantilevers,” *J. Vac. Sci. Technol. B Microelectron. Nanom. Struct.*, vol. 19, no. 2, p. 551, 2001.

[69] M. Imboden and P. Mohanty, “Dissipation in nanoelectromechanical systems,” *Phys. Rep.*, vol. 534, no. 3, pp. 89–146, 2014.

[70] B. Lassagne, D. Garcia-Sanchez, A. Aguasca, and A. Bachtold, “Ultrasensitive mass sensing with a nanotube electromechanical resonator,” *Nano Lett.*, vol. 8, no. 11, pp. 3735–3738, 2008.

[71] A. K. Huttel, G. A. Steele, B. Witkamp, M. Poot, L. P. Kouwenhoven, and H.

S. J. Van Der Zant, “Carbon nanotubes as ultrahigh quality factor mechanical resonators,” *Nano Lett.*, vol. 9, no. 7, pp. 2547–2552, 2009.

[72] N. Liu *et al.*, “Time-domain control of ultrahigh-frequency nanomechanical systems,” *Nat. Nanotechnol.*, vol. 3, no. 12, pp. 715–719, 2008.

[73] D. Garcia-Sanchez *et al.*, “Mechanical detection of carbon nanotube resonator vibrations,” *Phys. Rev. Lett.*, vol. 99, no. 8, pp. 1–4, 2007.

[74] V. Sazonova, Y. Yaish, H. Üstünel, D. Roundy, T. A. Arias, and P. L. McEuen, “A tunable carbon nanotube electromechanical oscillator,” *Nature*, vol. 431, no. 7006, pp. 284–287, 2004.

[75] R. B. Bhiladvala and Z. J. Wang, “Effect of fluids on the Q factor and resonance frequency of oscillating micrometer and nanometer scale beams,” *Phys. Rev. E - Stat. Nonlinear, Soft Matter Phys.*, vol. 69, no. 3 2, pp. 1–5, 2004.

[76] H. B. Peng, C. W. Chang, S. Aloni, T. D. Yuzvinsky, and A. Zettl, “Ultrahigh frequency nanotube resonators,” *Phys. Rev. Lett.*, vol. 97, no. 8, pp. 2–5, 2006.

[77] H. Jiang, M. F. Yu, B. Liu, and Y. Huang, “Intrinsic energy loss mechanisms in a cantilevered carbon nanotube beam oscillator,” *Phys. Rev. Lett.*, vol. 93, no. 18, pp. 1–4, 2004.

[78] A. K. Vallabhaneni, J. F. Rhoads, J. Y. Murthy, and X. Ruan, “Observation of nonclassical scaling laws in the quality factors of cantilevered carbon nanotube resonators,” *J. Appl. Phys.*, vol. 110, no. 3, p. 034312, 2011.

[79] S. Hutcherson and W. Ye, “On the squeeze-film damping of micro-resonators in the free-molecule regime,” *J. Micromechanics Microengineering*, vol. 14, no. 12, pp. 1726–1733, 2004.

[80] P. Li and Y. Fang, “A molecular dynamics simulation approach for the squeeze-film damping of MEMS devices in the free molecular regime,” *J. Micromechanics Microengineering*, vol. 20, no. 3, 2010.

[81] C. Chen *et al.*, “Nanoscale fluid-structure interaction: Flow resistance and energy transfer between water and carbon nanotubes,” *Phys. Rev. E - Stat. Nonlinear, Soft Matter Phys.*, vol. 84, no. 4, pp. 1–7, 2011.

[82] S. Sawano, T. Arie, and S. Akita, “Carbon nanotube resonator in liquid,” *Nano Lett.*, vol. 10, no. 9, pp. 3395–3398, 2010.

[83] F. Müller-Plathe, S. C. Rogers, and W. F. van Gunsteren, “Gas sorption and transport in polyisobutylene: Equilibrium and nonequilibrium molecular dynamics simulations,” *J. Chem. Phys.*, vol. 98, no. 12, pp. 9895–9904, 1993.

[84] S. J. Stuart, A. B. Tutein, and J. A. Harrison, “A reactive potential for hydrocarbons with intermolecular interactions,” *J. Chem. Phys.*, vol. 112, no. 14, pp. 6472–6486, 2000.

[85] J. Zhao, A. Buldum, J. Han, and J. P. Lu, “Gas molecule adsorption in carbon nanotubes and nanotube bundles,” *Nanotechnology*, vol. 13, no. 2, pp. 195–200, 2002.

[86] H. Zhan, Y. Gu, and H. S. Park, “Beat phenomena in metal nanowires, and their implications for resonance-based elastic property measurements,” *Nanoscale*, vol. 4, no. 21, p. 6779, 2012.